High-Resolution Initialization and Simulations of Typhoon Morakot (2009)

HIEP VAN NGUYEN AND YI-LENG CHEN

Department of Meteorology, University of Hawaii at Manoa, Honolulu, Hawaii

(Manuscript received 19 May 2010, in final form 4 January 2011)

ABSTRACT

A model self-bogus vortex is constructed by cycle runs using the Weather Research and Forecasting (WRF) model to provide high-resolution initial conditions for tropical cyclone (TC) simulations. The vortex after 1 h of model simulation is used to construct the vortex structure for the initial conditions for the next cycle run. After about 80 cycle runs, the TC structure is well adapted to the model employed and well adjusted to the given large-scale conditions.

Three separate simulations using three different initial conditions including global analysis (CTRL), the bogus package from WRF (WB), and the new initialization package (NT) are performed for Typhoon Morakot (2009). The NT scheme shows advantages in generating realistic vortex features including sea level pressure, winds, a warm core, and correct TC size with the meteorological fields away from the observed TC center consistent with the global analysis. The NT scheme also shows significant improvements in TC simulations including asymmetric structure, track, intensity, strength of low-level winds, radar reflectivity, and rainfall. For other runs, such as WB and CTRL, the unbalanced initial vortex needs to adjust to the changing environment during the first 2–3 days of model simulations, which is likely to have negative impacts on the track, intensity, and rainfall forecasts in most cases.

For all three different types of model initializations, the model is capable of simulating heavy orographic precipitation over southern Taiwan. However, with a better track forecast, only the NT run simulates the high-reflectivity band associated with the convergence zone between Morakot's circulations and the southwest monsoon off the southeast coast. In addition to Morakot's slow movement and relatively large size, Typhoons Goni and Etau were embedded within a moist monsoon gyre. The combined circulations associated with the monsoon gyre and tropical storms bring in moisture-laden flows toward the western slopes of southern Taiwan.

1. Introduction

Initialization of tropical cyclones (TC) in numerical models has been a challenging problem for many years. For TC track and intensity predictions, unfortunately, the tropical cyclone structure is usually not well represented in the model initial conditions because TCs form and develop over the open ocean where observations are few. In addition, the initial conditions for mesoscale models are interpolated from global analyses that may not have adequate resolution to resolve real TC structure, especially in the TC core area. The initial vortices associated with tropical cyclones from global analyses are usually too large and too weak compared to real vortices (Kurihara et al. 1993).

To improve the initial conditions for numerical TC forecasts, a vortex specification technique is usually used. The procedures include removing the poorly analyzed meteorological fields associated with TCs from the global analysis, constructing an empirical vortex or a bogus vortex (Iwasaki et al. 1987; Mathur 1991; Kurihara et al. 1993), and inserting the bogus vortex into the observed TC location. The bogus vortex has an intensity, size, and location close to observations. Techniques for TC initialization can be divided into three groups including 1) a bogus vortex constructed by model integration, 2) a bogus vortex constructed by analytic empirical functions, and 3) a bogus vortex constructed by three- (3DVAR) or four-dimensional variational data assimilation (4DVAR) with bogus data as one of the data sources.

One of the well-known TC initialization techniques in the first type of vortex initialization was developed by

Corresponding author address: Yi-Leng Chen, Dept. of Meteorology, School of Ocean and Earth Science and Technology, University of Hawaii at Manoa, Honolulu, HI 96822.
E-mail: yileng@hawaii.edu

DOI: 10.1175/2011MWR3505.1

Kurihara et al. (1993). In the technique, a bogus vortex is constructed by model integration. They suggested that a bogus vortex needs to satisfy three conditions including consistency in structure, similarity in structure to the real vortex, and compatibility with the numerical model in which it is inserted. The bogus vortex in Kurihara et al. (1993) is constructed with both symmetric and asymmetric components. The symmetric component is produced by integrating an axisymmetric version of the Geophysical Fluid Dynamics Laboratory (GFDL) hurricane model (Kurihara et al. 1990). The asymmetric component is constructed by integrating the nondivergent barotropic vorticity equation on a beta-plane using the initial conditions from the constructed symmetric flows (Ross and Kurihara 1992). Liu et al. (1997) used the fifth-generation Pennsylvania State University–National Center for Atmospheric Research (PSU–NCAR) nonhydrostatic Mesoscale Model (MM5) for a 48-h integration with the coarsest domain. Then, the integrated vortex from the coarsest domain at 48 h was extracted and implanted into the model initial conditions for all domains. Vortex initialization using model integration shows significant improvement in terms of the thermodynamic structure of the vortex and intensity forecasts (Kurihara et al. 1993; Liu et al. 1997; Wu et al. 2002).

In the second type of vortex initialization, bogus vortices are constructed from empirical functions of surface pressure and tangential wind (Fujita 1952; Holland 1980; Chan and Williams 1987; Iwasaki et al. 1987; Mathur 1991; Davis and Low-Nam 2001; Kwon and Cheong 2010). The bogus vortices then replace the vortices from the large-scale analysis. The method is able to reproduce many realistic features of hurricanes with significant improvement in track and intensity forecasts as compared to model forecasts without a bogus vortex (Davidson and Weber 2000; Kwon and Cheong 2010).

Vortex initialization by application of data assimilation is a recent technique for TC initialization. Zou and Xiao (2000) introduced a bogus data assimilation (BDA) scheme to initialize Hurricane Felix (1995) using the MM5 model with some success. By applying BDA, models generate initial conditions in such a way that all variables are forced to adjust to observations and a bogus low (Zou and Xiao 2000). Chou and Wu (2008) integrated the bogus vortex with the dropwindsonde data to produce better initial conditions. Compared with a no-vortex initialization, the vortex initialization by application of 3DVAR and 4DVAR with bogus data, including sea level pressure (SLP) and/or bogus wind profile (Zou and Xiao 2000; Pu and Braun 2001; Wu et al. 2006; Zhao et al. 2007; Zhang et al. 2007; Wang et al. 2008), shows significant improvements on TC structure, track, and intensity forecasts.

The island of Taiwan affects the track and intensity of TCs. From observations of 22 typhoons, Brand and Blelloch (1974) state that all typhoons in their sample start to weaken at about 12 h prior to landfall. Bender et al. (1985, 1987) suggest that the weakening of TCs is due to the advection of dry and low momentum air from Taiwan into the TC circulation. The advection reduces the supply of latent heat and kinetic energy both of which help the TCs to maintain their circulations. Interaction between TCs and Taiwan's terrain causes track deflection, as blocking effects change the upstream steering flows as well as TC circulations (Yeh and Elsberry 1993a,b; Bender et al. 1987). When a TC hits Taiwan, a secondary low usually forms in the lee side. The leeside low is induced by environmental flow in combination with downslope adiabatic warming associated with TC circulations (Wu and Kuo 1999; Wu 2001). The leeside low then may replace the original TC low resulting in the TC propagating twice as fast as the speed of the basic flow (Chang 1982). Jian et al. (2006) suggest that the replacement occurs as the original low is blocked by the Central Mountain Range (CMR); a part of the vorticity associated with the original low is transported horizontally across the CMR to the secondary low at the lee side. Finally, the upper-level vorticity remnant of the original low passes through the CMR and couples with the low-level secondary low to form a mature TC in the lee.

With a height over 3 km, the CMR plays an important role in the development of heavy rainfall due to the interaction between the TC and the terrain as the oceanic moisture-laden air is forced upslope by TC circulations (Wu et al. 2002). Strong orographic lifting is accompanied by significant latent heating in the lower atmosphere above the slopes (Wu et al. 2002). Over Taiwan, the locations of heavy rainfall associated with TCs are mainly controlled by orographic forcing and coastal convergence rather than a particular TC's rainband (Bender et al. 1985; Lin et al. 2002). Heavy rainfall can be more severe if TCs hit Taiwan and interact with the East Asian winter monsoon, as the convergence is enhanced by monsoon circulations (Wu et al. 2009). The rainfall distributions associated with TCs over Taiwan are strongly controlled by the relative locations of TC tracks over Taiwan (Cheung et al. 2008). It is suggested that with an accurate track forecast, model resolution and model depiction of Taiwan terrain control the simulated rainfall (Wu and Kuo 1999; Wu et al. 2002).

Previous studies confirm that TC initialization is required to produce better forecasts by mesoscale numerical models. In this work, a TC-initialization technique is constructed using the Weather Research and Forecasting model (WRF; Skamarock et al. 2005) cycle runs and applied to Typhoon Morakot (2009). Model simulations initialized by the new TC-initialization technique and global analysis data are then used to investigate the mechanism for a record-breaking rainfall event associated with Morakot (2009). Details about the TC-initialization technique are described in section 2. The model and data description are given in section 3. Some preliminary results from a case study based on Typhoon Morakot (2009) are presented in sections 4 and 5. Development of the typhoon vortex in the proposed TC initialization scheme is discussed in section 6. Factors contributing to the heavy rainfall related to Morakot are discussed in section 7. Summary and discussion are given in section 8.

2. Vortex initialization

One of the purposes of this work is to develop a new vortex initialization technique and compare it with the vortex bogus technique in the current WRF model. The bogus scheme in the current Advanced Research WRF model (ARW-WRF) is adapted from the same scheme (Davis and Low-Nam 2001) used in the MM5 model. The scheme includes two main steps. In the first step, the vortex from the global analysis is removed using relationships among nondivergent winds, the streamfunction, and the vorticity. With the assumption that the streamfunction and the vorticity of the vortex part vanish at large radii from the vortex center, the relationships among nondivergent wind, streamfunction, and vorticity result in a Laplace's equation with Dirichlet's boundary conditions. The equation is then solved by a spectral method to find the vortex part in the global analysis. In the second step, an empirical axisymmetric Rankine vortex is constructed and inserted into the observed location of the real vortex. Davis and Low-Nam (2001) suggest that the axisymmetric bogus vortex does not affect the storm motion at the time close to the initial time. In fact, the inserted axisymmetric bogus vortex induces asymmetric features via the beta effect, which would affect the simulated TC track.

In this work, a technique is developed to construct TC vortices in the model initial conditions using ARW-WRF. In the proposed technique, a model self-bogus vortex is constructed by the model cycle runs. During the cycle runs, only SLP is specified at the first time step of each cycle run by an empirical profile. We assume that 1) in a short period of time (<1 h) the TC moves but its structure does not change significantly; and 2) a TC's structure at the model initial time is a function of environmental conditions including SST, winds, temperature, relative humidity, and other meteorological variables, which also do not significantly change in each cycle run. The model is first integrated for a short period of time dt ($dt < 1$ h), with the prescribed SLP associated with the tropical cyclone at the model initial time t_0. Next, the vortex structure after dt integration is used to construct a new vortex at the initial time t_0 of the next cycle run at the initial observed TC center while the large-scale variables are the same as those from global analysis at t_0. Then the model is integrated again for dt. The above two-step cycle run is repeated until the current TC has the minimum SLP ($P_{\min}$) and the maximum wind speed $V_{\max}$ at the initial time close to the observed values with a preset criterion or after a fixed number of cycle runs N. Usually, N is about 80. As will be shown later, the repeated two-step cycle run will assure that the initial vortex is well adapted to the model used and is in quasi-equilibrium with the given large-scale environment from the global analysis and the prescribed SLP associated with the TC.

To obtain the bogus TC, the following processes are applied for every variable F at the beginning of each cycle run:

$$F^V_{c+1,t_0,x,y,z} = F^V_{c,t_0,x,y,z} + f^V_{c,t_0,x,y,z} \quad c = 1, \ldots, N, \quad (1)$$

where, x, y, z denote spatial coordinates; F^V_c and F^V_{c+1} are the vortex parts of variable F at cycle c and $c + 1$ at the model initial time t_0; and f^V_c is the difference in the vortex part of variable F at cycle c between the initial time and initial time plus dt. In this case, dt is 60 min. Here N is the number of cycle runs.

a. Vortex separation

The cycle processes only apply to the vortex part and within a radius of R from the TC center. The R can be selected as the radius of 15 m s^{-1} wind from the best-track data or a fixed experimental number.

A variable, F, is first decomposed into the vortex component F^V and the environment component F^E:

$$F = F^V + F^E, \quad (2)$$

and following the modified methods of Kurihara et al. (1993) F^E is defined as

$$\begin{aligned} \overline{F}^E_{i,j} &= F_{i,j} + K_m(F_{i-q_n,j} + F_{i+q_n,j} - 2F_{i,j}) \\ F^E_{i,j} &= \overline{F}^E_{i,j} + K_m(\overline{F}^E_{i,j-q_n} + \overline{F}^E_{i,j+q_n} - 2\overline{F}^E_{i,j}), \end{aligned} \quad (3)$$

where

$$\begin{aligned} q_n &= \left[\frac{111\cos(\phi_0)}{n\Delta}\right] \quad n = 1, 2, 4, \ldots, M, \\ M &= \left[\frac{111\cos(\phi_0)}{\Delta}\right], \end{aligned} \quad (4)$$

$$K_m = \left[\frac{1}{2}\left(1 - \cos\frac{2\pi}{m}\right)^{-1}\right] \quad m = 2, 3, 4, 2, 5, 6, 7, 2, 8, 9, 2. \quad (5)$$

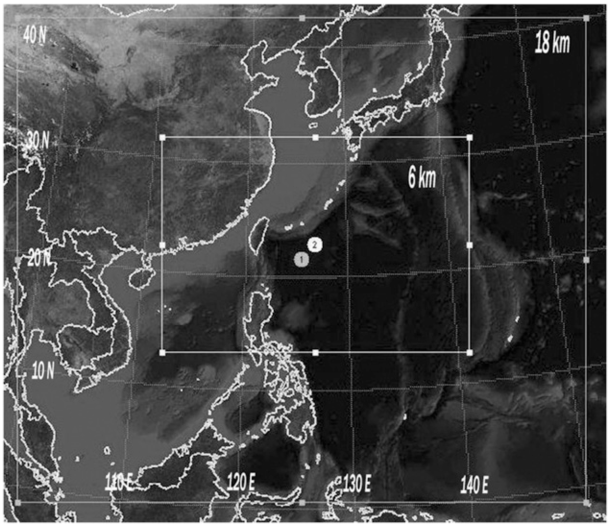

FIG. 1. The two employed domains.

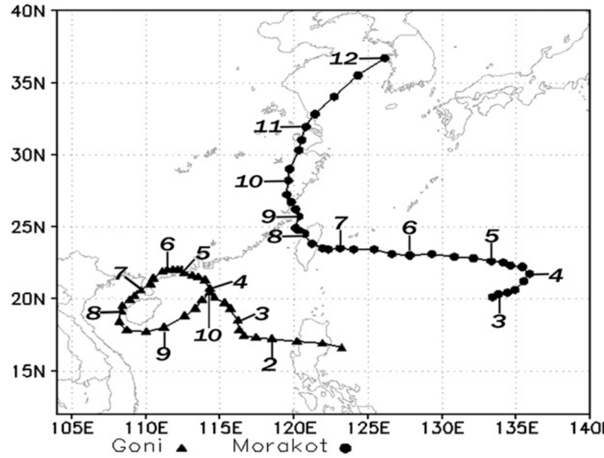

FIG. 2. Observed tracks of (top right) Typhoon Morakot (circle) and (bottom left) Typhoon Goni (triangle) are marked every 6 h. The numbers next to the observed TC locations indicate the observed time at 0000 UTC of the days in August 2009.

In this work, the integer number q_n is added to the original equation to make (3) applicable for all horizontal resolutions smaller than 100 km in the WRF model, where φ_0 is the latitude of the observed TC center, Δ is the horizontal grid resolution in kilometers for each domain, and [ ] denotes the operator to round an argument to the nearest whole number. To apply (3), (4), and (5) for real data, with each value of n, successive applications of (3) are performed with values of m as suggested by Kurihara et al. (1993) in which m varies as 2, 3, 4, 2, 5, 6, 7, 2, 8, 9, and 2. With n equal to 1, the modified processes (3), (4), and (5) have almost the same effect as the original method of Kurihara et al. (1993), in which all waves with a wavelength between about 100 km to 900 km are completely removed. Other values of n in (4) will remove all waves with wavelengths shorter than 100 km.

The vortex component is defined as the difference between the environment and the total field using (2). The difference could include small-scale environmental noises in addition to the vortex. However, according to Kurihara et al. (1993), the magnitude of the small-scale environmental noise is small compared with the vortex.

b. The prescribed sea level pressure associated with a TC vortex

During the cycle runs that generate the bogus vortex, the only information needed for this technique is the SLP distribution at the model initial time, t_0. Three parameters are used to construct a modified Fujita's surface pressure including minimum pressure $P_{\min}$, radius of maximum wind $R_{\max}$, and radius R beyond which the values of all variables are the same as in the global analysis. The prescribed SLP, $P(r, \theta)$, has a maximum gradient at $R_{\max}$, and has the same value as the global analysis at radius R. A modified Fujita's equation (Fujita 1952) is applied for each grid point within a distance of R from the observed TC center:

$$P(r,\theta) = P_0(\theta, R) - [1 - W(r, R)]\frac{P_0(\theta, R) - P_{\min}}{\sqrt{1 + \left(\frac{r}{R_{\max}}\right)^2}}, \qquad (6)$$

where $P_{\min}$ is the observed minimum SLP, r is the distance from the grid point to the observed TC center, and $P_0(\theta, R)$ is the SLP from the global analysis at radius R. Note that $P_0(\theta, R)$ is a function of the azimuthal angle θ allowing the asymmetric structure of the TC to develop in the initial vortex during the cycle runs. Because TC structure over land is strongly affected by terrain, the cycle runs should be only applied to TCs with a distance from the TC center to the nearest landmass larger than R.

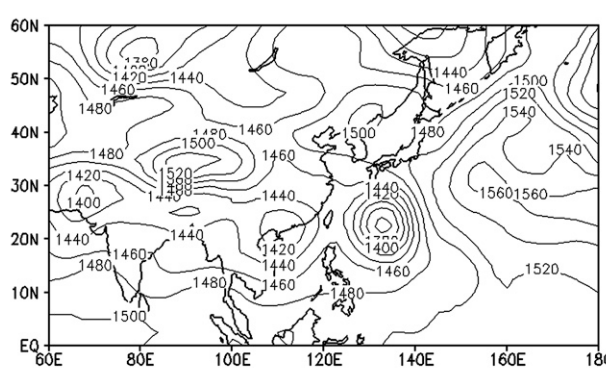

FIG. 3. FNL 850-hPa geopotential height (m) at 0000 UTC 5 Aug 2009.

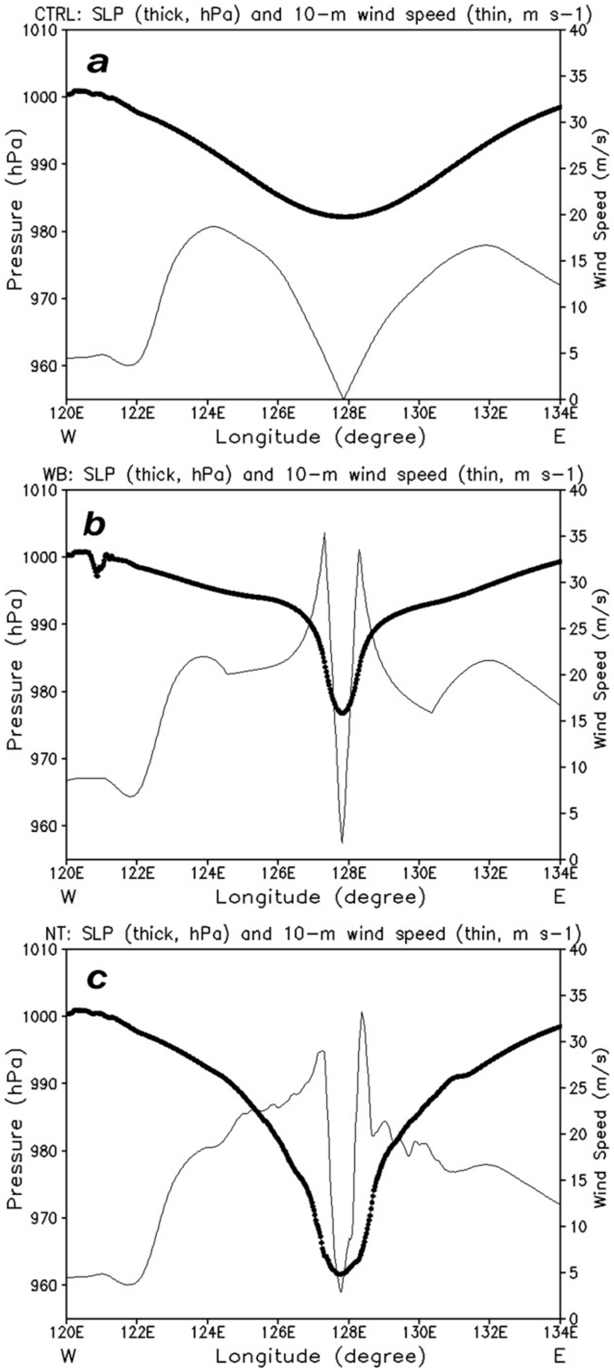

FIG. 4. East–west cross section along the TC center (23.0°N) of initial SLP (thick contour, hPa) and 10-m wind speed (thin contour, m s^{-1}) for the (a) CTRL, (b) WB, and (c) NT runs at 0000 UTC 6 Aug 2009.

The $W(r, R)$ is the matching function (Kwon and Cheong 2010) and is given as follows:

$$W(r) = e^{-[(r-R)/\alpha R]^2}, \tag{7}$$

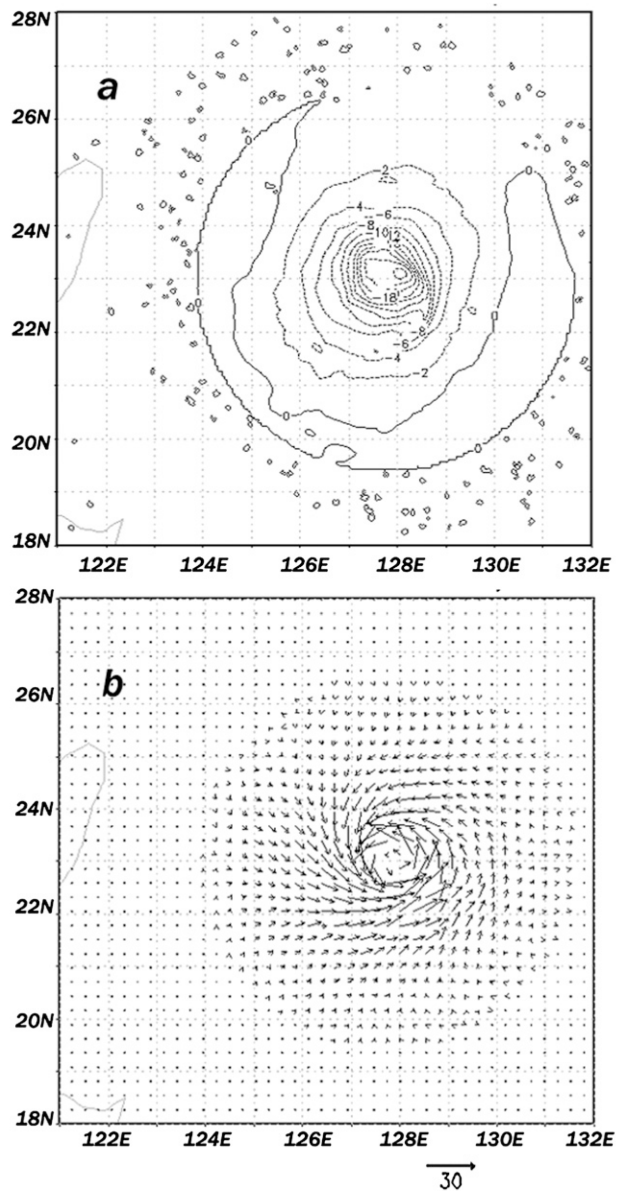

FIG. 5. The difference in vortex part between the analysis and after vortex initialization for the NT run for (a) SLP (hPa) and (b) 10-m wind vector (m s^{-1}).

where $\alpha = 0.4$ is the shape parameter.

c. Cycle runs

Apply (2) for all variables at both t_0 and $t_0 + dt$ to obtain the first term on the right-hand side of (1). The second term on the right-hand side of (1), the difference in vortex part f_s^V at cycle c between t_0 and $t_0 + dt$, is computed by

$$f^V_{c,t_0,x,y,z} = W_{x,y}F^V_{c,t_0,x,y,z} + (1 - W_{x,y})F^V_{c,t_0+dt,x+dx,y+dy,z}, \tag{8}$$

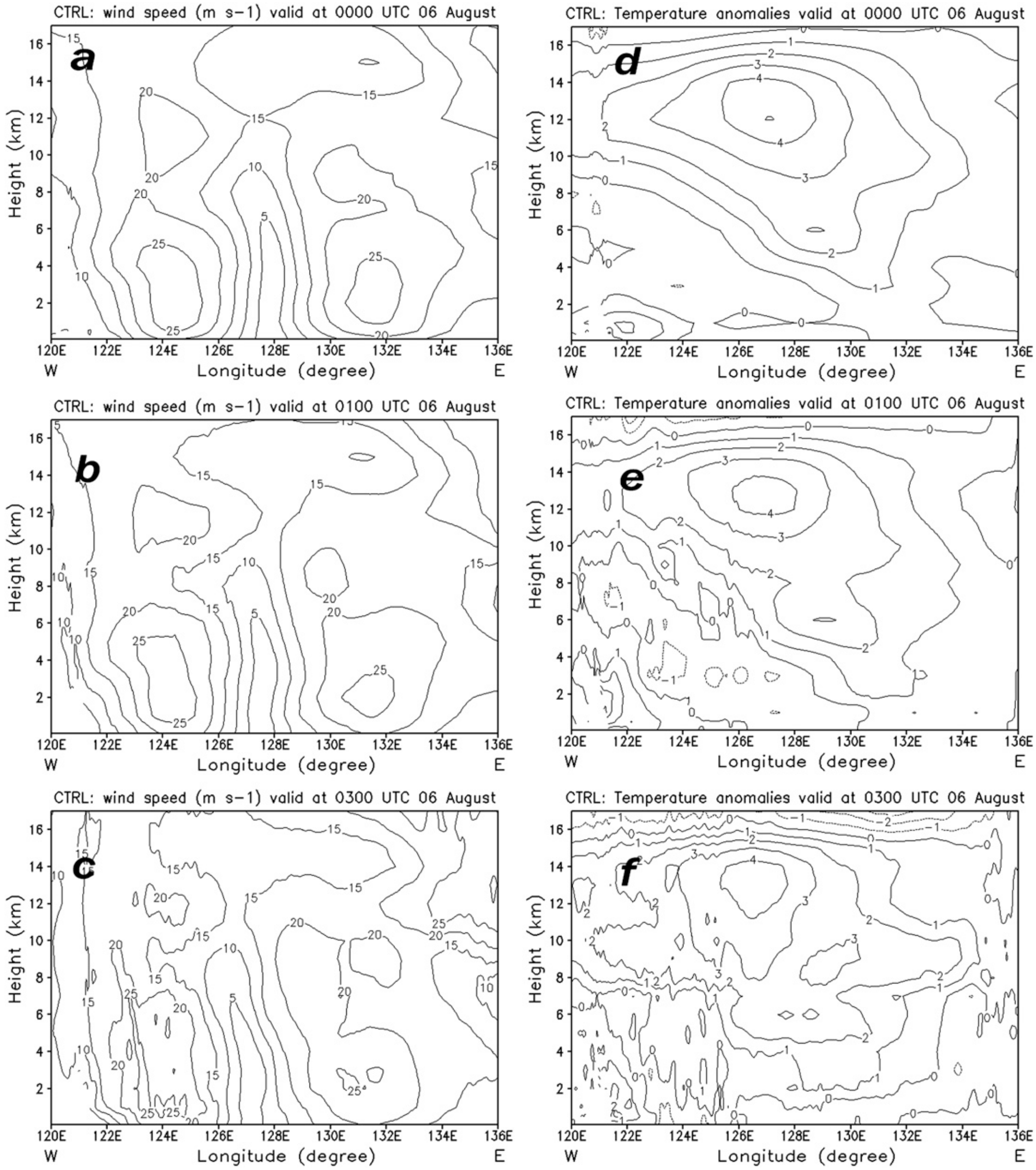

FIG. 6. Longitude–vertical cross sections through the TC center, for the CTRL run, of wind speed (m s^{-1}, interval 5 m s^{-1}) at (a) 0000, (b) 0100, (c) 0300 UTC and temperature anomalies (K, interval of 1 K) from the environment at the same height at (d) 0000, (e) 0100, and (f) 0300 UTC 6 Aug 2009.

where dx and dy are the differences between the observed TC center at t_0 and the simulated TC center at $t_0 + dt$ in the x and y directions, respectively.

Bender et al. (1993) show that models develop unrealistic grid-scale variations during integration. To remove the noise, they suggest that smoothing and desmoothing at appropriate time-step intervals should be performed. The following operations (Bender et al. 1993) are applied for the vortex component every five cycles:

$$F^V_{x,y} = (1 - 4\upsilon)F^V_{x,y} + 2\upsilon(F^V_{x-dx,y} + F^V_{x+dx,y}) \quad \text{and}$$
$$F^V_{x,y} = (1 - 4\upsilon)F^V_{x,y} + 2\upsilon(F^V_{x,y-dy} + F^V_{x,y+dy}), \qquad (9)$$

where $\upsilon = 0.25$ for smoothing, and $\upsilon = -0.28$ for desmoothing. As suggested by Bender et al. (1993), moisture variables are only smoothed, without desmoothing, to avoid generating unrealistic values.

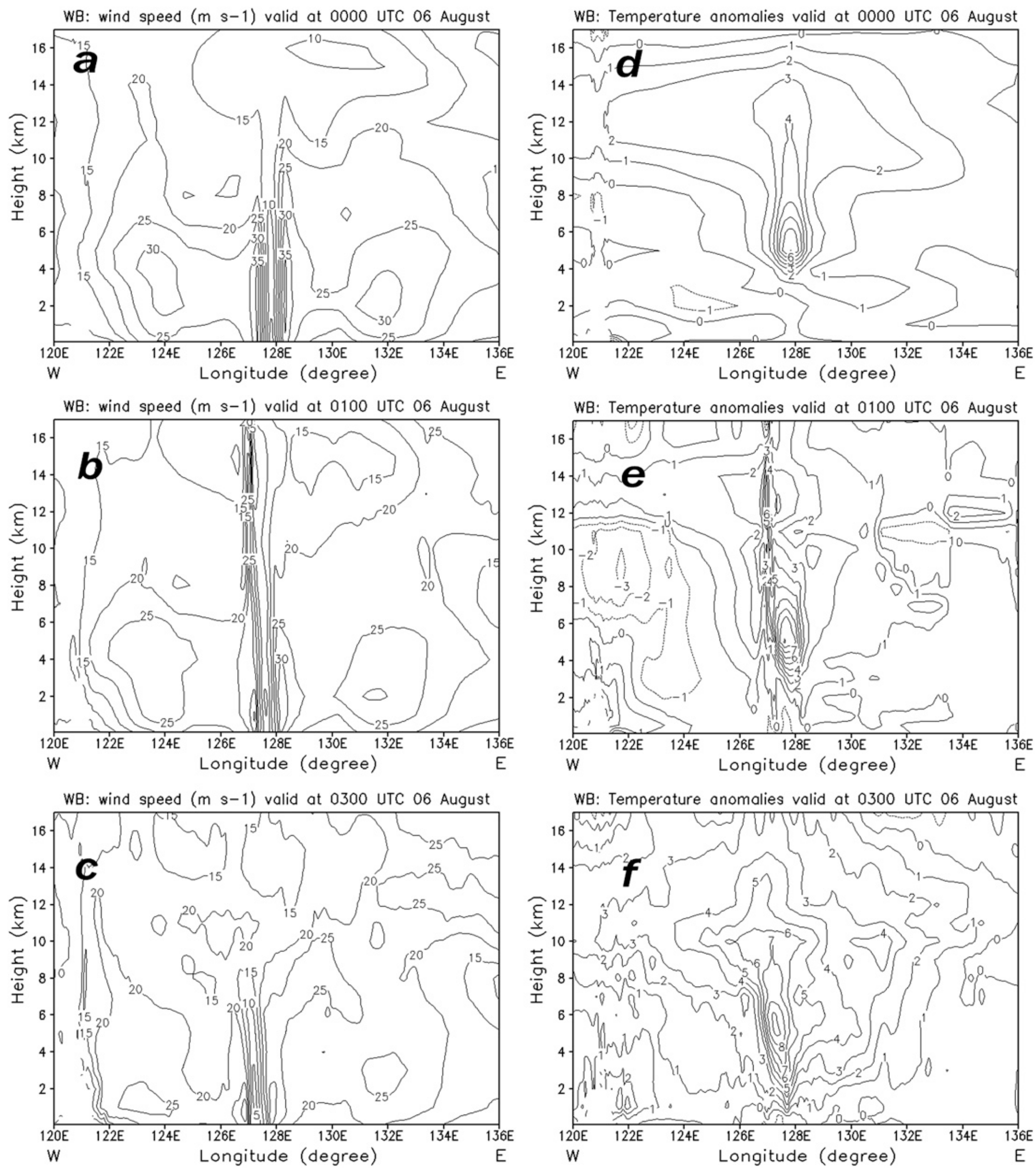

FIG. 7. As in Fig. 6, but for the WB run.

3. Data and model descriptions

The WRF modeling system is a nonhydrostatic, three-dimensional primitive equation model (Skamarock et al. 2005) and is currently used for both research and operational forecasts. The model configuration in this research includes a Ferrier microphysics scheme (Ferrier et al. 2002), a Rapid Radiative Transfer Model scheme (Mlawer et al. 1997) for longwave radiation, the Dudhia scheme (Dudhia 1989) for shortwave radiation, the Monin–Obukhov similarity scheme (Monin and Obukhov 1954) for surface layer physics, the Yonsei University scheme (Noh et al. 2003) for planetary boundary layer physics, and the Betts–Miller–Janjic scheme (Janjic 1994, 2000) for cumulus parameterization. An advanced land surface model (Chen and Dudhia 2001) is employed using the land surface update procedures introduced by Zhang et al. (2005). The terrain height, land use, green fraction, and vegetation cover, as well as radar data, were provided by the Central Weather Bureau (CWB), Taiwan. Rainfall data over Taiwan Island are from the Automatic Rainfall and Meteorological Telemetry System (ARMTS) stations (Chen et al. 2007). The estimated rainfall from the Tropical Rainfall Measuring Mission (TRMM) satellite

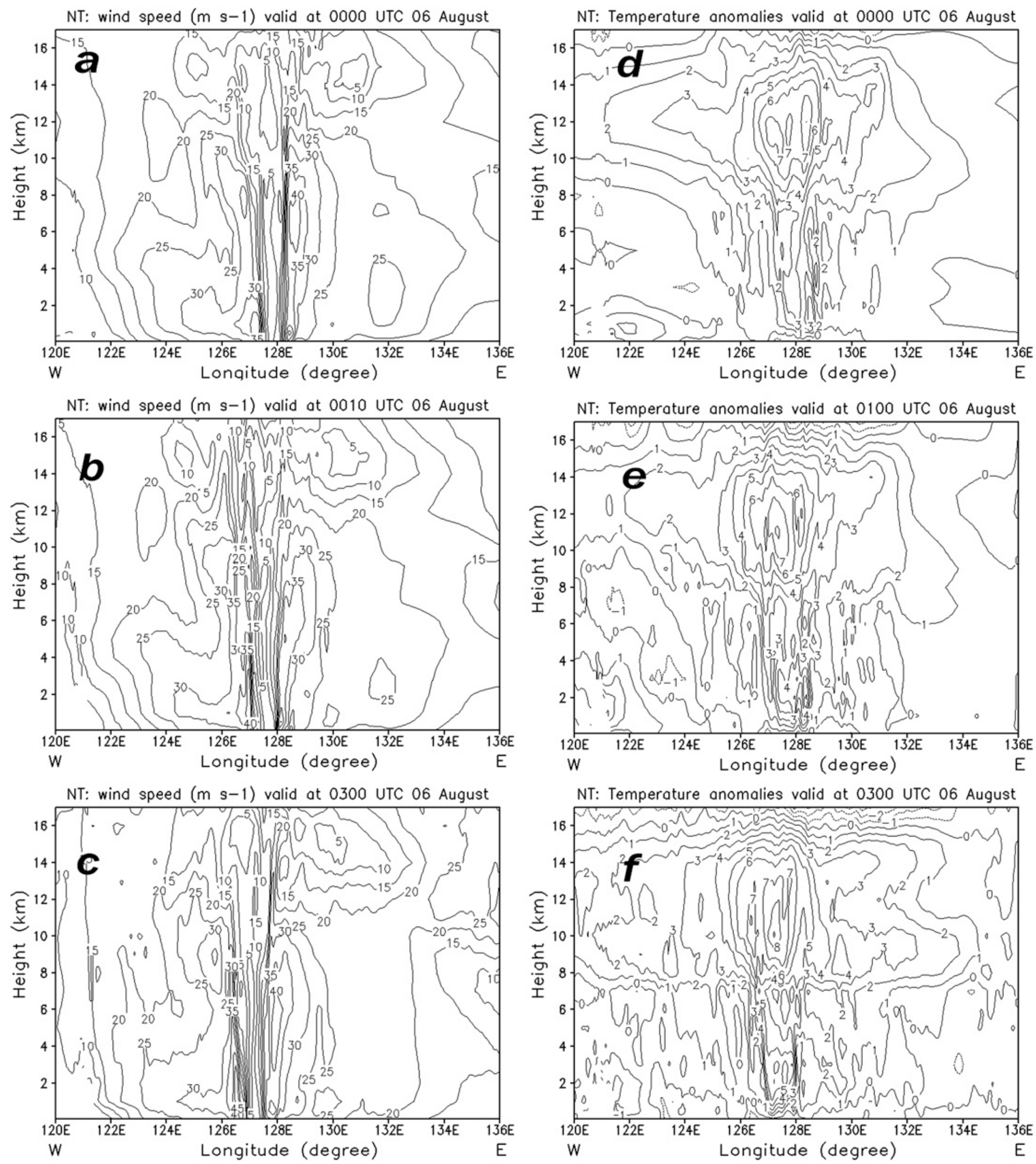

FIG. 8. As in Fig. 6, but for the NT run.

Microwave Imager (TMI) with horizontal resolution of about 25 km is used to validate simulated rainfall at early hours of model simulation over the ocean.

For the simulation of Typhoon Morakot, two nested domains are employed in the model with two-way nesting. The domains have horizontal resolutions of 18 and 6 km, and horizontal dimensions of 311 × 256 and 505 × 343, respectively (Fig. 1). There are 28 vertical levels from the surface to the 50-hPa level. Initial and lateral boundary conditions for the model are from the National Centers for Environmental Prediction (NCEP) Final Analyses (FNL) with one-degree horizontal resolution. The best-track and intensity data are from the Japan Meteorological Agency (JMA; see online at http://agora.ex.nii.ac.jp/digital-typhoon). The simulated accumulated rainfall, winds, and radar reflectivity are compared with observations for verification.

4. Simulations of Typhoon Morakot initialized at 0000 UTC 6 August

The vortex initialization technique presented in section 2 is coded and incorporated with WRF model V3.1.1. In this section, preliminary results for a 3-day simulation of

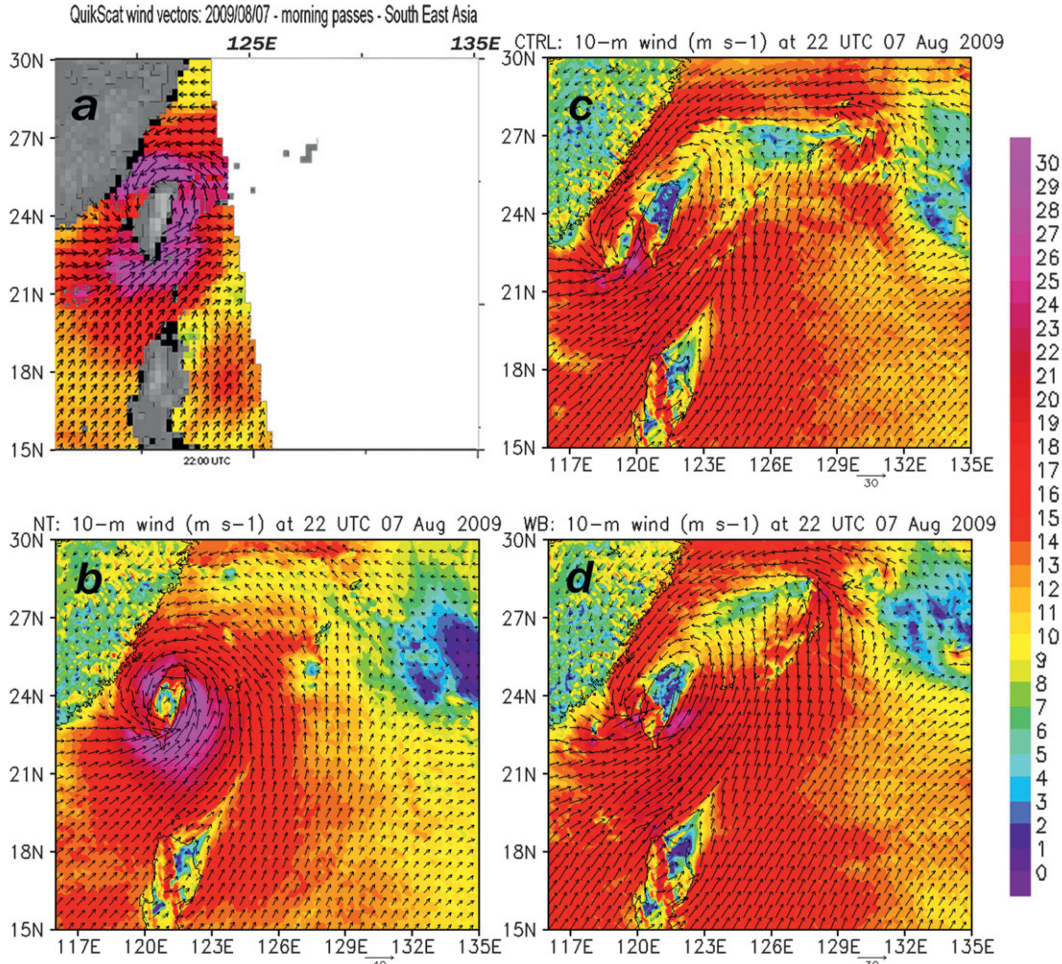

FIG. 9. Horizontal distribution of 10-m winds (m s^{-1}) for (a) QuikSCAT observations and 46-h simulations for the (b) NT, (c) CTRL, and (d) WB runs at 2200 UTC 7 Aug 2009.

Morakot initialized at 0000 UTC 6 August are presented. Three different types of initial conditions, including those from global reanalysis data (CTRL), from the bogus package of WRF (WB), and from the new initialization package (NT) are performed for comparison. Other than the differences in the initial conditions, the WRF model is configured as described in section 3 for all runs. In this section, it will be shown that the new TC initialization scheme (NT) is capable of generating a TC-like structure in the core area that is reasonably well balanced with the large-scale fields, including outward tilt of the eyewall, maximum winds near the eyewall, weak winds in the eye, and a warm core. We also would like to show that with a well-balanced realistic vortex at the model initial time, the NT run is able to capture rainfall and radar reflectivity patterns associated with the eyewall and asymmetric rainbands starting from the early hours of model simulation with better simulations of the storm intensity and track. Furthermore, we also will show the impact of better track simulation in the model on the simulated localized heavy rainfall distributions over Taiwan.

a. *Overview of Typhoon Morakot*

The best track from the JMA shows that Morakot was formed on 2 August 2009. It reached its peak intensity, with winds of 150 km h^{-1} (a category-2 hurricane), on early 7 August and made landfall over Taiwan on late 7 August. It stayed over Taiwan for about a day and then moved over the Taiwan Strait for about a day after which it made landfall over the China coast on 9 August. The typhoon weakened and dissipated on 11 August (Fig. 2).

During 5–9 August, Morakot was embedded within a monsoon gyre (Hong et al. 2010), defined as a large monsoon cyclonic vortex, with a size of about 2500 km (Lander, 1994). The FNL 850-hPa geopotential height at 0000 UTC 5 August (Fig. 3) shows that to the west of

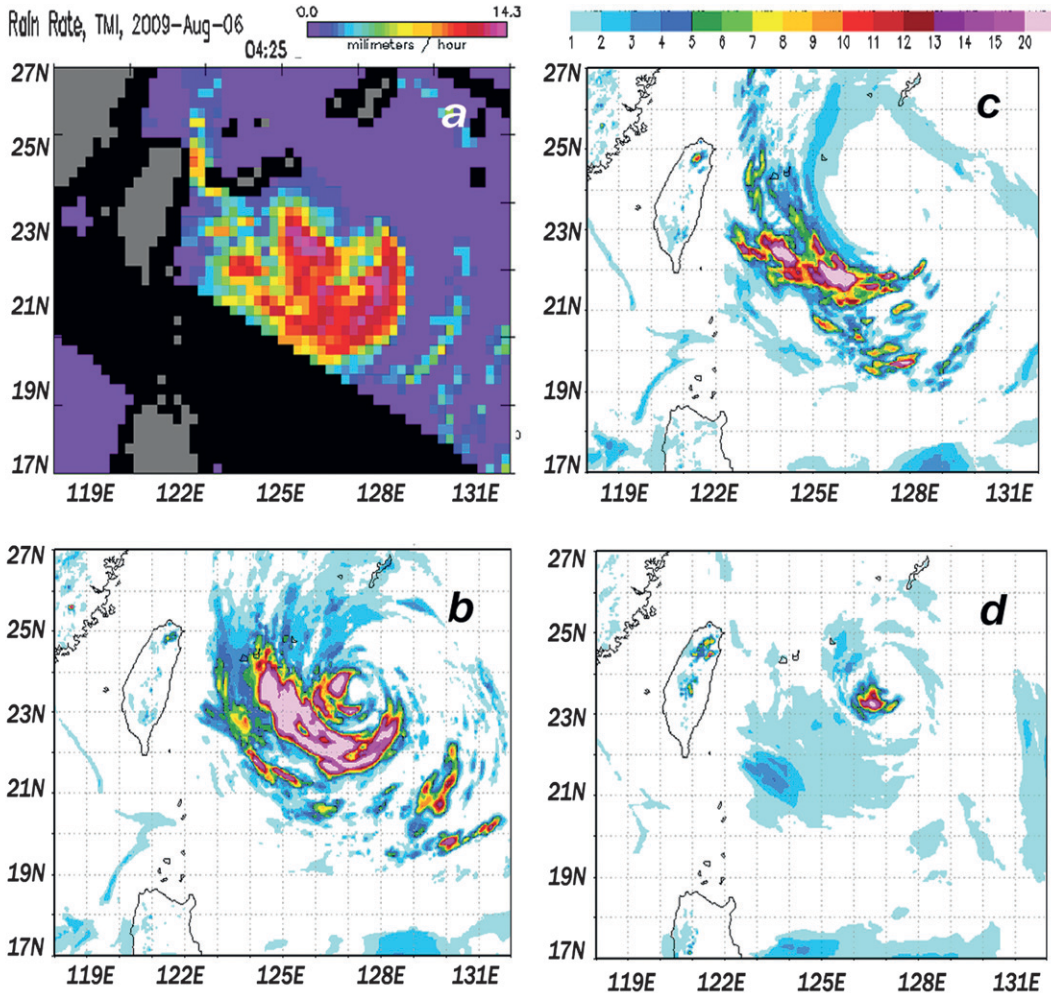

FIG. 10. (a) TMI satellite estimated rain rate (mm h^{-1}) at 0430 UTC 6 Aug 2009 and 1-h accumulated rainfall from 0400 to 0500 UTC 6 Aug 2009 for the (b) NT, (c) CTRL, and (d) WB runs.

Morakot, there is tropical storm Goni south of Hong Kong, China. Typhoon Goni formed on 1 August near the Philippines, made landfall over the south China coast on 5 August, moved back over the open ocean around Hainan Island, and dissipated on 10 August (Fig. 2). A high pressure cell is also located to the northeast of Morakot (Fig. 3).

Although Typhoon Morakot was only a category-2 typhoon, it was the wettest typhoon affecting Taiwan on records, with a maximum total accumulated rainfall of ~2777 mm (109.3 in.). Morakot was also the deadliest typhoon in Taiwan history. There were more than 500 casualties, with losses totaling more than \$237 million (U.S. dollars).

b. TC initialization

To assess the impact of the new TC initialization technique on the model initial conditions and forecast, the model is initialized at 0000 UTC 6 August, about 36 h before Morakot made landfall over Taiwan. At the model initial time, Morakot reached a minimum sea level pressure of 965 hPa and obtained a maximum wind speed of 33.5 m s^{-1}. The TC center was located at about 23.0°N, 127.8°E with the radius for gale winds (wind speed > 17.1 m s^{-1}) at approximately 650 km. The fixed size of the bogus vortex in the WRF bogus package is 400 km. To focus on improving data in the TC core and to make comparison with the WB runs, for the Morakot case, R in (6) is also chosen as 400 km.

The TC intensity from the global analysis is too weak, with a minimum SLP only about 982 hPa (Fig. 4a). Although the WB scheme can initialize the vortex with a much lower SLP (Fig. 4b) as compared to the CTRL run, the minimum SLP (~978 hPa) is still much higher than the observed value of 965 hPa. For the NT run, the initial minimum SLP (Fig. 4c) is close to the best-track data with

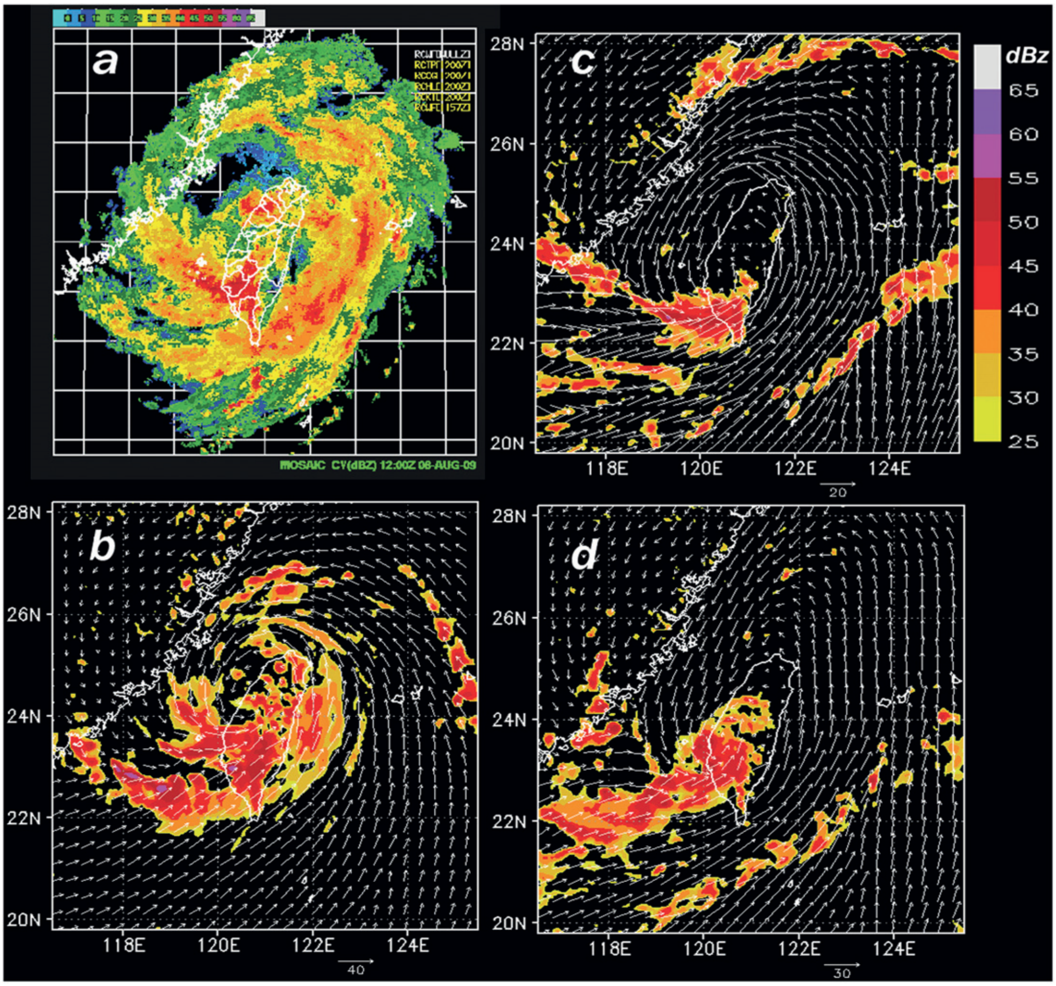

FIG. 11. Horizontal distribution of radar reflectivity (dBZ) at 1200 UTC 8 Aug 2009 for (a) observed and simulated radar reflectivity of more than 25 dBZ for the (b) NT, (c) CTRL, and (d) WB runs after 60 h of integrations.

a minimum SLP of about 965 hPa. In addition, both the initial SLP and wind speed (Fig. 4c) in the NT run at a radius larger than about 400 km away from the TC center are identical with the global analysis in Fig. 4a. Meanwhile, wind speeds in the WB run (Fig. 4b) are higher than in the CTRL run (Fig. 4a) at large radius. Two marked changes in wind speeds, one near 124.5°N and the other near 130.5°N, are also visible in the WB run (Fig. 4b). The 10-m wind speeds in the NT run reach the observed value of 33.5 m s^{-1} (Fig. 4c). In contrast, the maximum speed in the CTRL run is only about 20 m s^{-1}. Figure 5a shows the differences in SLP between the CTRL and NT runs. The largest difference in the SLP (~20 hPa) occurs near the TC center. The NT run generates a cyclonic 10-m wind field with wind speeds much stronger than in the reanalysis (Fig. 5b).

To investigate the consistency in TC structure, vertical–longitude cross sections of temperature anomalies from the environment at the same height and wind speeds at the initial time, 1 and 3 h after the initial time for the CTRL, WB, and NT runs are shown. In the CTRL run (Fig. 6) at the initial time, the analysis vortex shows that the location of strongest wind speeds is about 2.5° away from the TC center (Fig. 6a). After 3 h of simulation, the problem of too large an eye size is still unchanged (Fig. 6c). The analysis vortex shows a warm core, with the warmest temperature anomaly, of over 5 K, at a height of about 12 km (Fig. 6d). The warm core at the initial time is located about 1° away from the observed TC center. Right after an hour of simulation, the analysis vortex starts to develop some small-scale features (Figs. 6b,e).

For the WB run, the inserted bogus vortex is neither well adjusted to the large-scale fields nor well adapted by the model. The strong wind speeds in the area at the height of about 2 km near the eyewall at 128°E decrease from over 35 m s^{-1} at the initial time (Fig. 7a) to about 30 m s^{-1} within just an hour of simulation (Fig. 7b). The

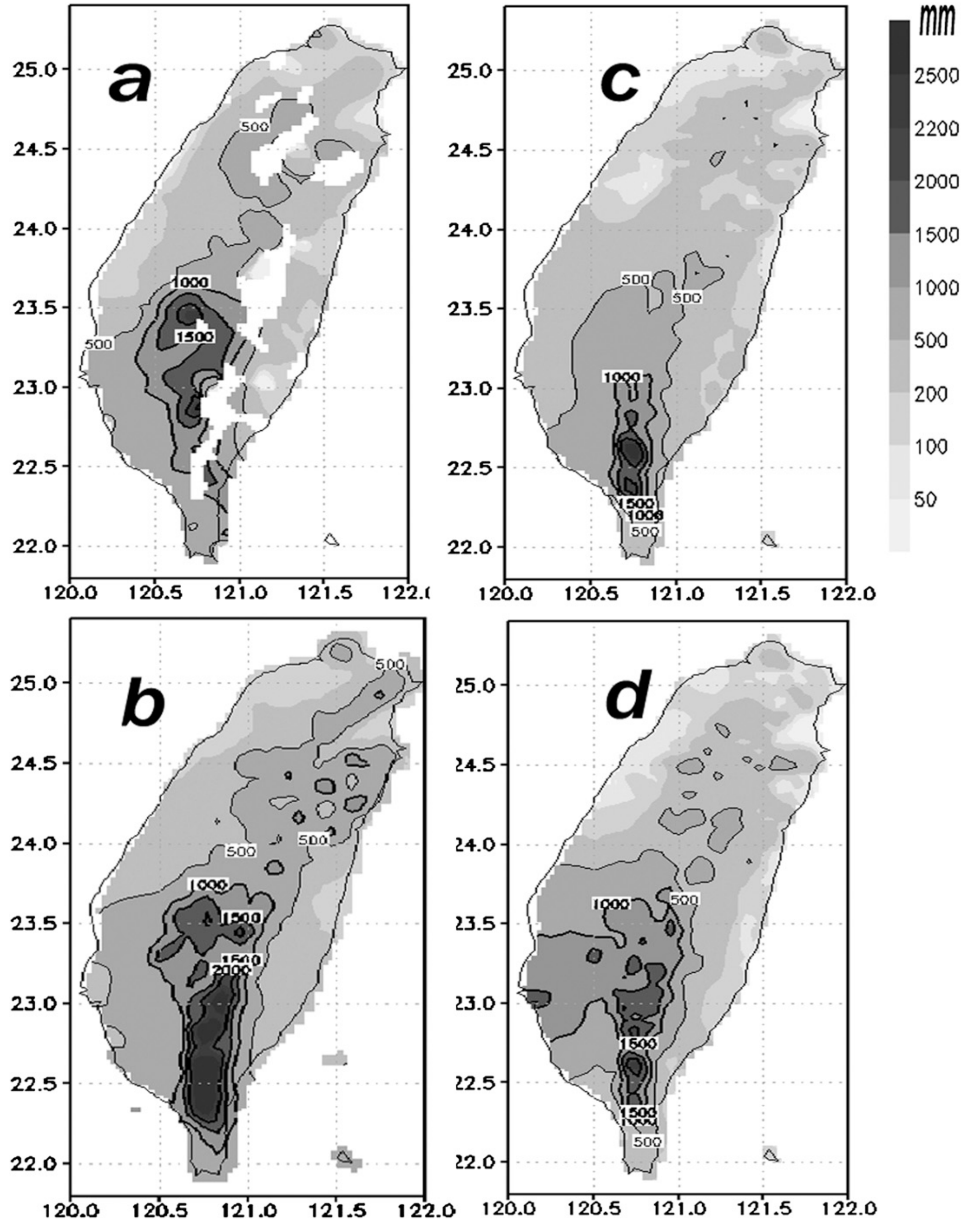

FIG. 12. The 3-day rainfall accumulation (mm) from 0000 UTC 6 Aug to 0000 UTC 9 Aug 2009 for (a) observation and 6-km simulation with the (b) NT, (c) CTRL, and (d) WB runs.

area of wind speeds over 30 m s^{-1} near 132°E in the initial conditions (Fig. 7a) disappears after 3 h of simulation (Fig. 7c). Wind speeds in the WB run at large radii are notably stronger than in the CTRL run (Figs. 6a and 7a). The stronger wind speeds at large radii in the WB run than in the CTRL run may affect the steering flow and may have negative effects on track simulation in the WB run. The altitude of the maximum warm core, at about 5 km above the surface (Fig. 7d), is too low and unrealistic as compared with the global analysis. In fact, from the observations of Hurricane Hilda (1964), Hawkins and Rubsam (1968) showed that the TC warm core is located in the upper troposphere at ~250 hPa. Because of the incorrect warm-core altitude, the warm core in the WB

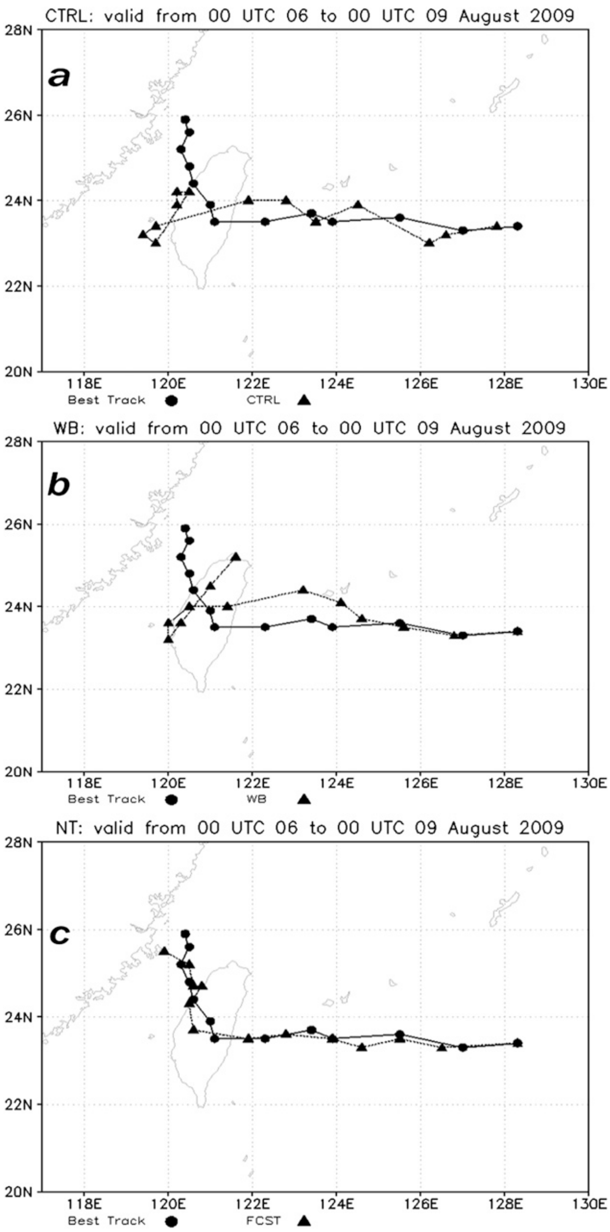

FIG. 13. Best track (solid line with circle) and simulated track (dashed line with triangle) for the (a) CTRL, (b) WB, and (c) NT runs, valid from 0000 UTC 6 Aug to 0000 UTC 9 Aug 2009. The model is initialized at 0000 UTC 6 Aug 2009. The TC tracks are marked every 6 h.

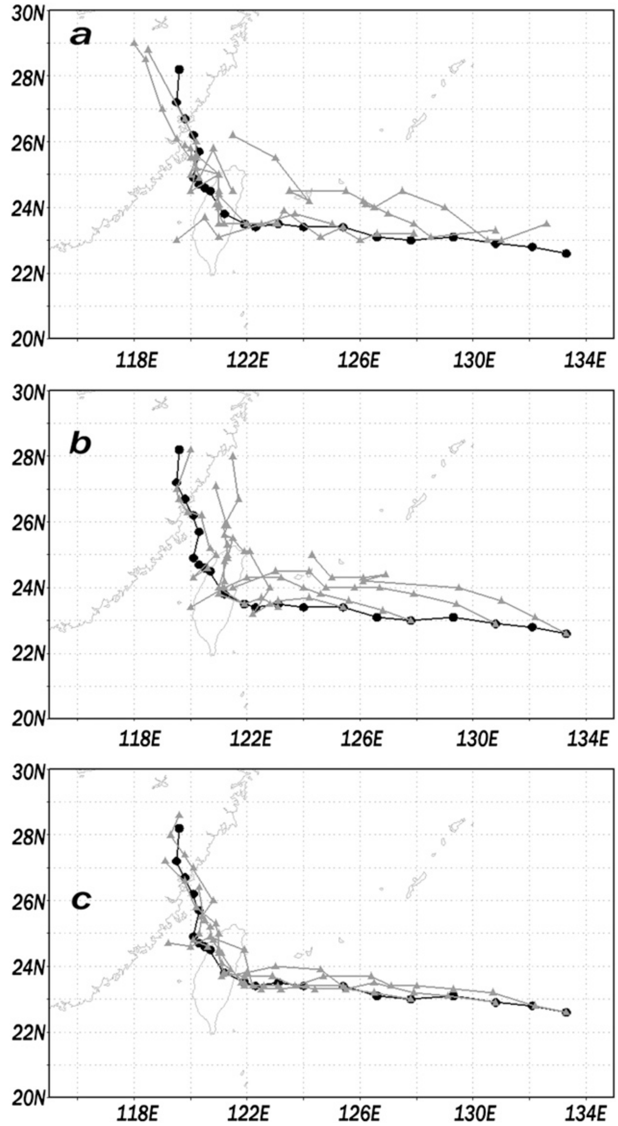

FIG. 14. Best track (circle) and 48-h simulated tracks (triangle) for all seven 48-h runs initialized every 12 h from 0000 UTC 5 Aug to 0000 UTC 8 Aug 2009 for the (a) CTRL, (b) WB, and (c) NT runs.

run starts to adjust to higher altitude after just an hour of simulation (Fig. 7e). After 3 h of simulation, a warm core developed at a higher altitude (Fig. 7f).

At the initial time, the NT run is able to generate a TC-like wind structure in the TC core area (Fig. 8a) including maximum winds near the eyewall, weak winds in the eye, and tilting of the eyewall with height. At radii larger than 400 km from the TC center, the initial winds in the CTRL run (Fig. 6a) and in the NT run (Fig. 8a) are identical. After 3 h of simulation, the vortex generated with the NT scheme does not have significant adjustments as the initial TC vortex has already been reasonably well adapted to the model used, and well adjusted to the large-scale environment and prescribed SLP associated with the TC vortex. Wind speeds (Figs. 8b,c) do not decrease as in the case of the WB scheme. The strong wind speeds at about the 1-km altitude near 126°E increase slightly from about 40 m s^{-1} at the initial time (Fig. 8a) to about 45 m s^{-1} after 3 h of simulation (Fig. 8c). Observations show that after 0000 UTC 6 August 2009, Typhoon Morakot was intensifying. The NT scheme generates a vortex with a warm core at about

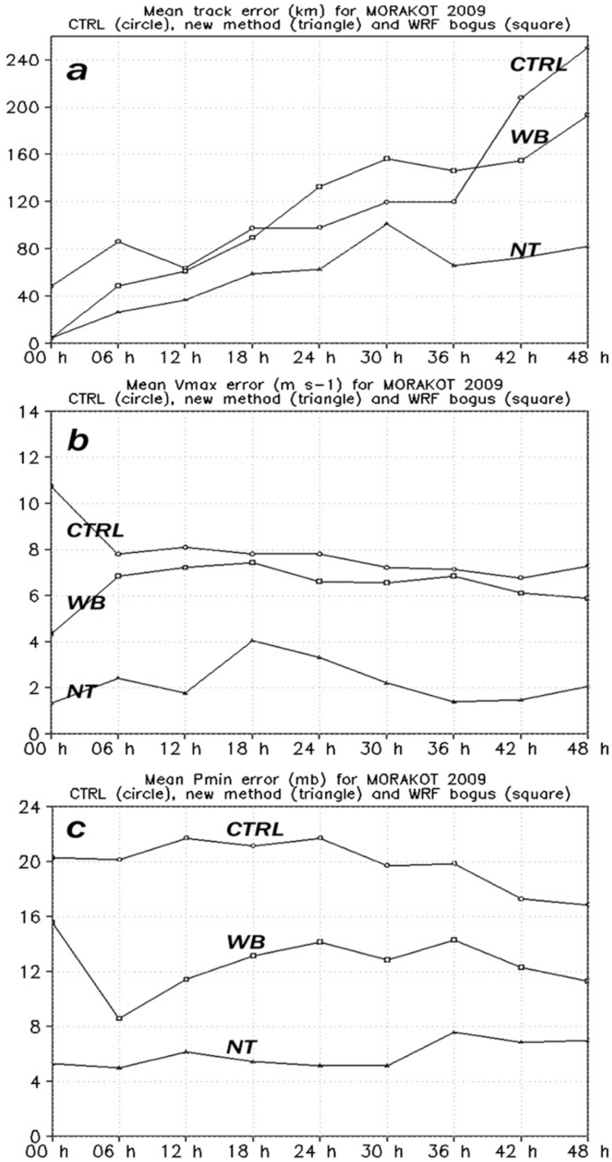

FIG. 15. Mean absolute errors for (a) track (km), (b) maximum wind speed (m s^{-1}), and (c) minimum SLP (hPa) for the CTRL (circle), WB (square), and NT (triangle) runs.

12 km (Fig. 8d), which is about the same height as in the global analysis (Fig. 6d), but about 2 K warmer. In addition, the warm core is located right above the observed TC center. After 3 h of simulation, the temperature anomaly structure does not have significant changes (Figs. 8e,f). The warm core still keeps its altitude at about 12 km. No significant adjustments of the TC structure in the NT run in the first few hours indicate that the vortex generated by the NT scheme is well adapted to the model employed and well adjusted to the given large-scale conditions.

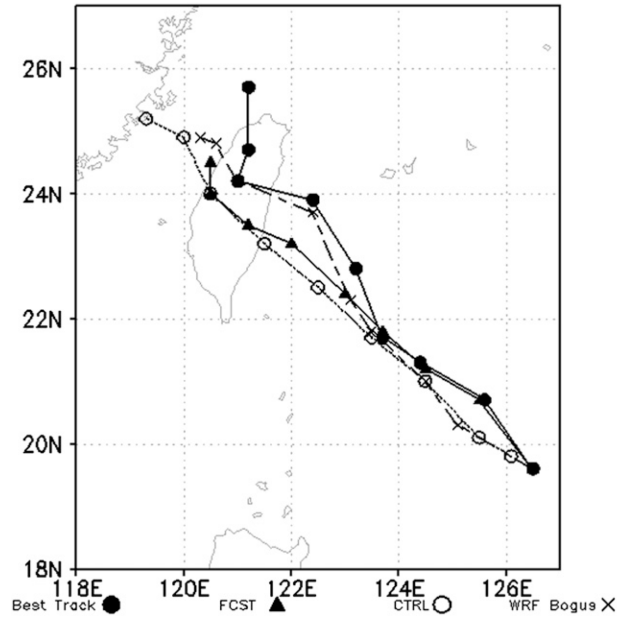

FIG. 16. Best track (solid line with circle) and simulated track for NT (solid line with triangle), CTRL (short-dashed line with open circle), and WB (long-dashed line with cross) runs for Typhoon Jangmi (2008), valid from 0000 UTC 27 Sep to 0000 UTC 29 Sep 2008. The model is initialized at 0000 UTC 27 Sep 2008. The TC tracks are marked every 6 h.

c. Model simulations

The simulated 10-m winds for these 3 runs are compared to available QuikSCAT wind observations (Fig. 9). After 46 h of simulation, without a TC initialization scheme, the CTRL run fails to simulate the strong winds in the core area (Fig. 9c). For the WB run, the model is able to better simulate 10-m winds (Fig. 9d), as compared to the CTRL run (Fig. 9c), even though the strong winds near the eyewall are still much weaker than in the QuikSCAT observations (Fig. 9a). In the NT run, although the area of wind speeds greater than 25 m s^{-1} near the TC eyewall (Fig. 9b) is still smaller than in observations (Fig. 9a), the simulated winds are superior to those from both the CTRL and WB runs. Compared to the WB and the CTRL runs, the strong winds in the core area of the NT run (Fig. 9b) are much closer to QuikSCAT observations (Fig. 9a).

Among the three types of model initializations, only the NT run is capable of generating reasonable TC-induced rainfall in the early hours of the simulation (Fig. 10). After 5 h of integration, only the NT run can reasonably generate rainfall associated with rainbands and the eyewall (Fig. 10b). The asymmetric rainfall pattern of the TC is simulated in the NT run (Fig. 10b) in agreement with satellite rainfall estimation (Fig. 10a). In Fig. 10, hourly rainfall accumulation with the NT run is over 20 mm, meanwhile the maximum estimated rain rate from the

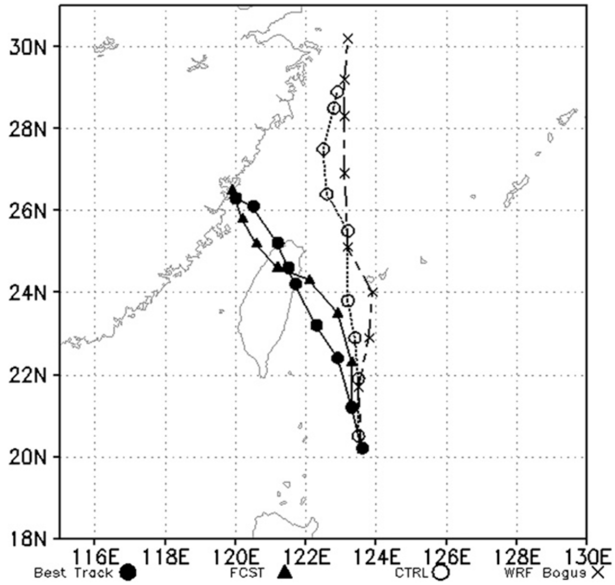

FIG. 17. Best track (solid line with circle) and simulated track for the NT (solid line with triangle), CTRL (short-dashed line with open circle), and WB (long-dashed line with cross) runs for Typhoon Kalmaegi (2008), valid from 1200 UTC 16 Jul to 1200 UTC 18 Jul 2008. The model is initialized at 1200 UTC 16 Jul 2008. The TC tracks are marked every 6 h.

TMI satellite is about 14 mm h^{-1}. The differences may be due to model overestimation of rainfall. It also may be due to the fact that the resolution of satellite data, of about 25 km, is too coarse to capture intensive convective cells. Viltard et al. (2006) reported that the TMI-estimated rainfall can have errors from 30% to 60%. The CTRL run can simulate some rainfall at relatively large radii (Fig. 10c); however, the rainfall simulation is very poor near the TC center. The rainfall simulation from the WB run (Fig. 10d) is the worst among the three runs, with almost no rain in the entire model domain.

At 1200 UTC 8 August, after 60 h of simulation, the simulated radar reflectivities in these three runs show significant differences (Fig. 11). Both the observed (Fig. 11a) and the simulated reflectivities from the NT run (Fig. 11b) show large areas of high radar reflectivities (>25 dBZ) associated with rainbands and the eyewall. In contrast, both the CTRL (Fig. 11c) and WB runs (Fig. 11d) simulated not well-organized radar reflectivities related to Morakot. Although the NT run underestimates radar reflectivity over the open ocean southeast of Taiwan, of the three sensitivity tests, only the NT run can simulate the observed band of high reflectivity near 23.5°N to the southwest of Taiwan (Figs. 11a,b).

Figure 12a shows that there are two local maxima in the 3-day (0000 UTC 6 August – 0000 UTC 9 August) observed rainfall of over 2000 mm over Taiwan. One located at 23.5°N, 120.7°E, the other located at 22.8°N, 120.8°E. After landfall, the simulated Morakot in the CTRL run moves to the open ocean southwest of Taiwan, whereas the best-track data show that Morakot moves toward the open ocean northwest of Taiwan (Fig. 13a). The simulated axis of the southwest flow, as a combination of storm circulations and southwest monsoon flow, shifts southward (Fig. 11c) as compared with what was observed. As a result, the CTRL run underestimated rainfall over central and northern Taiwan (Fig. 12c). In the WB run, the simulated Morakot stays over central Taiwan for over a day after landfall (Fig. 13b) resulting in an overestimation of rainfall over the southwestern plain of Taiwan with a local maximum at 23°N, 120.2°E (Fig. 12d). Rainfall over central and northern Taiwan is slightly underestimated in the WB run (Fig. 12d). With a better simulated track (Fig. 13c), the simulated rainfall over central and northern Taiwan in the NT run (Fig. 12b) is better than in both the CTRL (Fig. 12c) and WB (Fig. 12d) runs. The simulated rainfall in the NT run (Fig. 12b) reproduces both local rainfall maxima of over 2000 mm as found in the observations located at 23.5°N, 120.7°E and 22.8°N, 120.8°E, respectively (Fig. 12a). Over the southern end of the CMR, all runs show higher simulated rainfall maxima (Figs. 12b–d) as compared to observations (Fig. 12a). Note that there are no rain gauges over the high mountains of southern Taiwan (Fig. 12a) where the maximum rainfall axis is simulated. Furthermore, there are uncertainties in rainfall simulations at high horizontal resolutions and in the regions of complex terrain as rainfall amount may be dependent on the representation of convection in the model and boundary layer parameterization (Wu et al. 2002). With a horizontal resolution of 6 km, the convective updrafts and cells are smaller than the grid spacing. The model may not be able to resolve fundamental aspects of precipitation processes as the moist-laden southwest flow impinges on the CMR.

5. Sensitivity tests of 48-h simulations during 5–10 August

When the TC center is located less than 400 km from the nearest coast (from 0000 UTC 7 August onward), no cycle runs are performed for the NT run. In this case, the simulated vortex at 12 h from the previous NT run, initialized 12 h earlier, is used as a bogus vortex for the current simulation. Prior to 0000 UTC 7 August, the TC initialization described in section 2 is used. The model is initialized every 12 h from 0000 UTC 5 August to 0000 UTC 8 August for a total of seven 48-h simulations. The last run ended at 0000 UTC 10 August. Seven 48-h simulations are also performed for both the CTRL and WB runs during the same period. These 48-h simulations

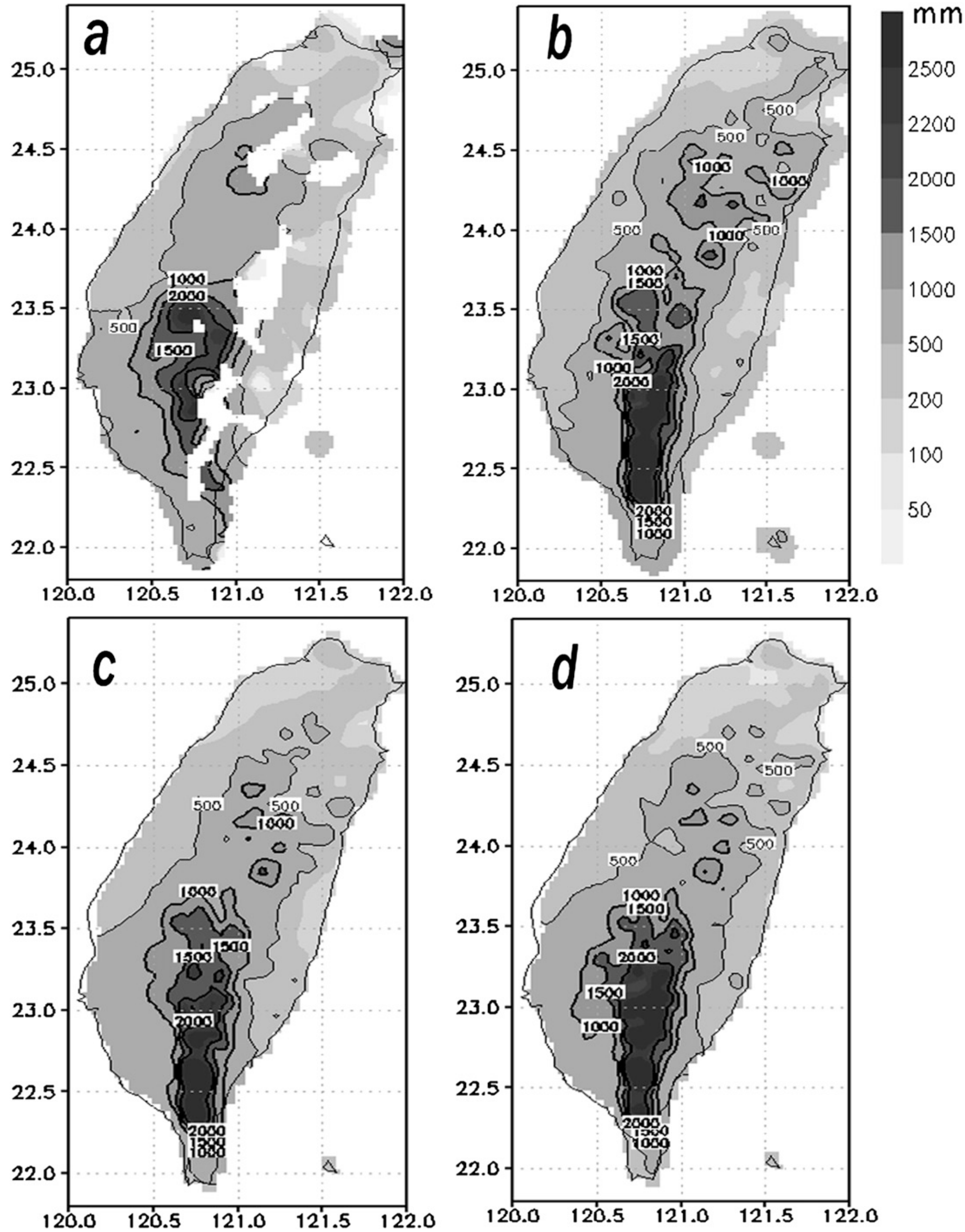

FIG. 18. The 5-day rainfall accumulation (mm) from 0000 UTC 5 Aug to 0000 UTC 10 Aug 2009 over Taiwan from (a) observations and 6-km simulations computed from 12 to 36 h of each simulation for the (b) NT, (c) CTRL, and (d) WB runs.

are used to compute the error statistics for the simulated track, intensity, and minimum SLP for all three runs (CTRL, WB, and NT). In addition, two additional runs, including a weak storm (e.g., Kalmaegi 2008) and a strong storm (e.g., Jangmi 2008), are also conducted to show that superior performance of the NT run is also valid for these cases, especially for the weak storm case.

Track simulations with these three different types of initial conditions for all seven runs are shown in Fig. 14. Among the three different types of initial conditions, the

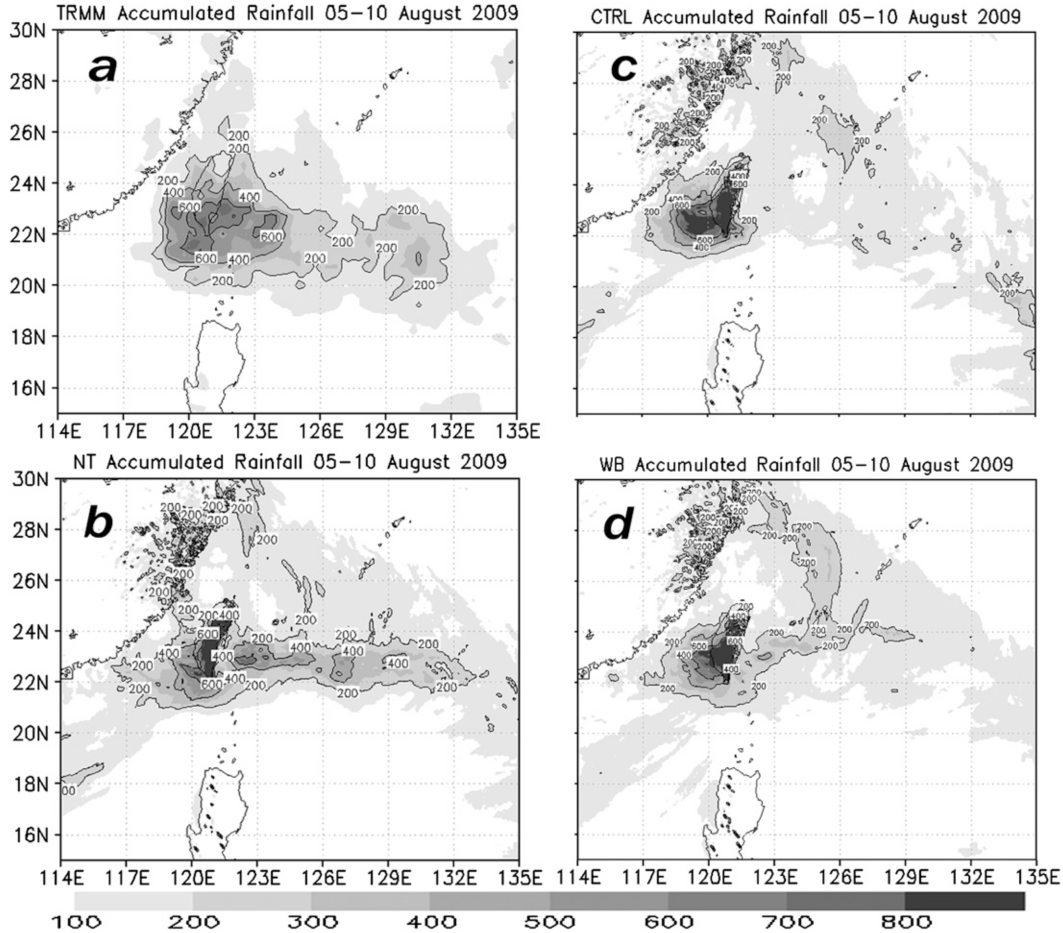

FIG. 19. The 5-day rainfall accumulation (mm) from 0000 UTC 5 Aug 2009 to 0000 UTC 10 Aug 2009 over Taiwan and the adjacent oceans from (a) TRMM satellite observations and 6-km simulations from the (b) NT, (c) CTRL, and (d) WB runs.

track forecast for Morakot is the best in the NT run (Figs. 14 and 15a). Within 48 h of simulation, the largest track error in the NT run is about 100 km. On the other hand, the values are 190 and 250 km in the CTRL and WB runs, respectively (Fig. 15a). The mean 24-h track errors for the seven runs are 100, 130, and 60 km for the CTRL, WB, and NT runs, respectively. The mean 48-h track errors are 250, 190, and 80 km for the CTRL, WB, and NT runs, respectively (Fig. 15a).

The NT run shows a significant improvement in the intensity forecast compared with the other two schemes. The mean 24-h maximum absolute wind speed errors are about 8, 6.5, and 3.5 m s^{-1} for the CTRL, WB, and NT runs, respectively (Fig. 15b). The mean 48-h maximum absolute wind speed errors are about 7, 6, and 2 m s^{-1} for the CTRL, WB, and NT runs, respectively (Fig. 15b). For the WB run, even though the maximum wind speed is close to the observed value at the model initial time, the wind speed decreases dramatically to values comparable to those in the CTRL after 6 h of integration (Fig. 15b). After 6 h, the WB run does not show notable advantages in simulating maximum wind speed compared to the CTRL run. This problem may be due to the inconsistency between the bogus vortex from the WB run and the environmental fields at the model initial time. Mean absolute SLP errors at 24 and 48 h of simulation in the NT run are about ⅓ and ½ of that in the CTRL and WB runs, respectively (Fig. 15c).

The NT scheme is used to simulate tracks of two other typhoons that hit Taiwan in 2008 to assess how the NT scheme works for other cases. Typhoon Jangmi (2008), a category-5 typhoon, and Typhoon Kalmaegi (2008), a category-1 typhoon, are selected. For each typhoon, a 48-h simulation, initialized about 36 h before the typhoon makes landfall over Taiwan, is performed. For Jangmi, the model is initialized at 0000 UTC 27 September 2008. Figure 16 shows that simulated tracks with different initial conditions are not significantly different for this strong

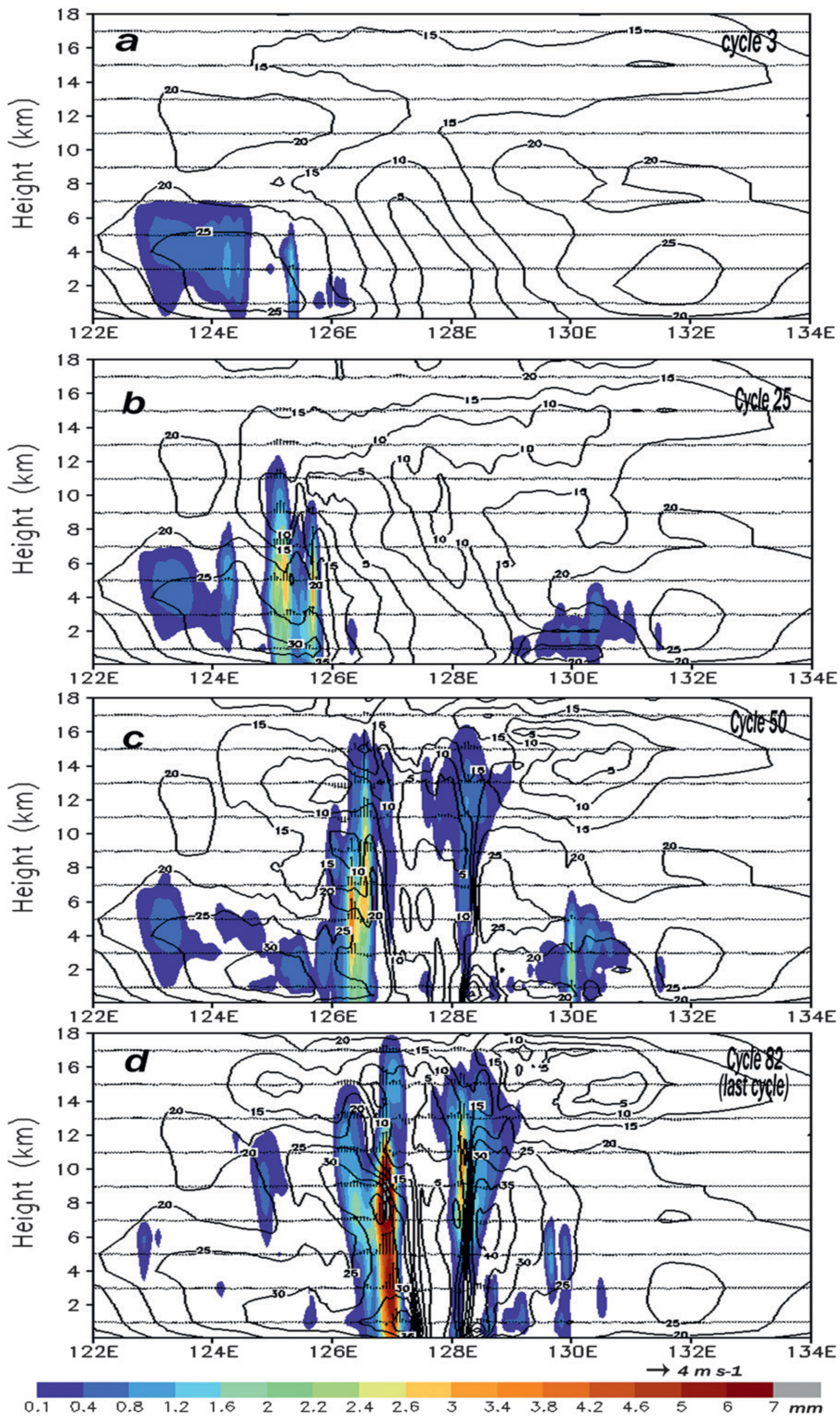

FIG. 20. Horizontal wind speed (contour, m s^{-1}) at 0000 UTC 6 Aug 2009, vertical wind vector (vector, m s^{-1}), and total condensate mixing ratio (g kg^{-1}) at 0100 UTC 6 Aug 2009 during the run for Morakot (2009) for cycle number (a) 3, (b) 25, (c) 50, and (d) 82 (the last cycle).

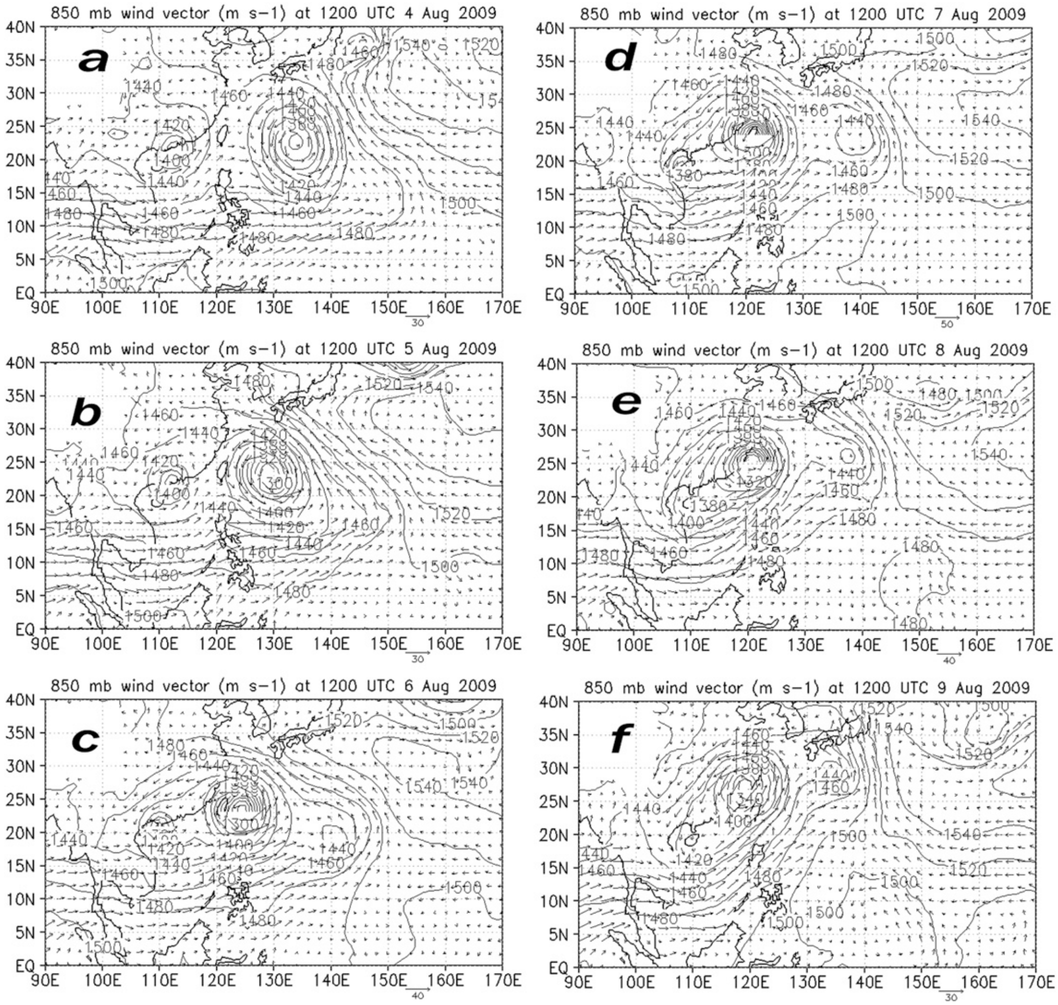

FIG. 21. FNL analysis of 850-hPa winds (m s^{-1}) and geopotential height (m) at 1200 UTC (a) 4, (b) 5, (c) 6, (d) 7, (e) 8, and (f) 9 Aug 2009.

typhoon case. For Typhoon Kalmaegi, the weak typhoon case, the model is initialized at 1200 UTC 16 July 2008. Both the CTRL and WB runs fail to simulate Kalmaegi making landfall over Taiwan (Fig. 17). Only the NT run successfully simulates the landfall time of Typhoon Kalmaegi with good track simulation (Fig. 17).

The 5-day observed and simulated rainfall accumulations over Taiwan from 0000 UTC 5 August to 0000 UTC 10 August for Typhoon Morakot are shown in Fig. 18. The 5-day simulated rainfall is computed from rainfall accumulation from 12 to 36 h of each simulation. Because simulations are performed every 12 h, the rainfall during the overlapping 12-h period between the two successive simulations is averaged. The simulated rainfall from 0000 to 1200 UTC 5 August and from 1200 UTC 9 August to 0000 UTC 10 August is extracted from the corresponding single simulation without averaging. Over the open ocean, the NT run produces better rainfall accumulations than the other two runs when compared with rainfall estimated from the TRMM satellite data (Fig. 19) because the track, intensity and tropical cyclone structure are better simulated by the NT run. Nevertheless, all the runs are able to simulate heavy orographic rainfall over southwest Taiwan with a maximum value over 2500 mm (Fig. 18). It is apparent that large-scale conditions and orographic lifting are crucial for the record-breaking rainfall associated with Morakot over Taiwan. This problem will be investigated further in section 7.

6. Development of the typhoon vortex in the NT scheme

For initialization of Morakot at 0000 UTC 6 August 2009, it takes 82 cycles for the NT run to produce a vortex

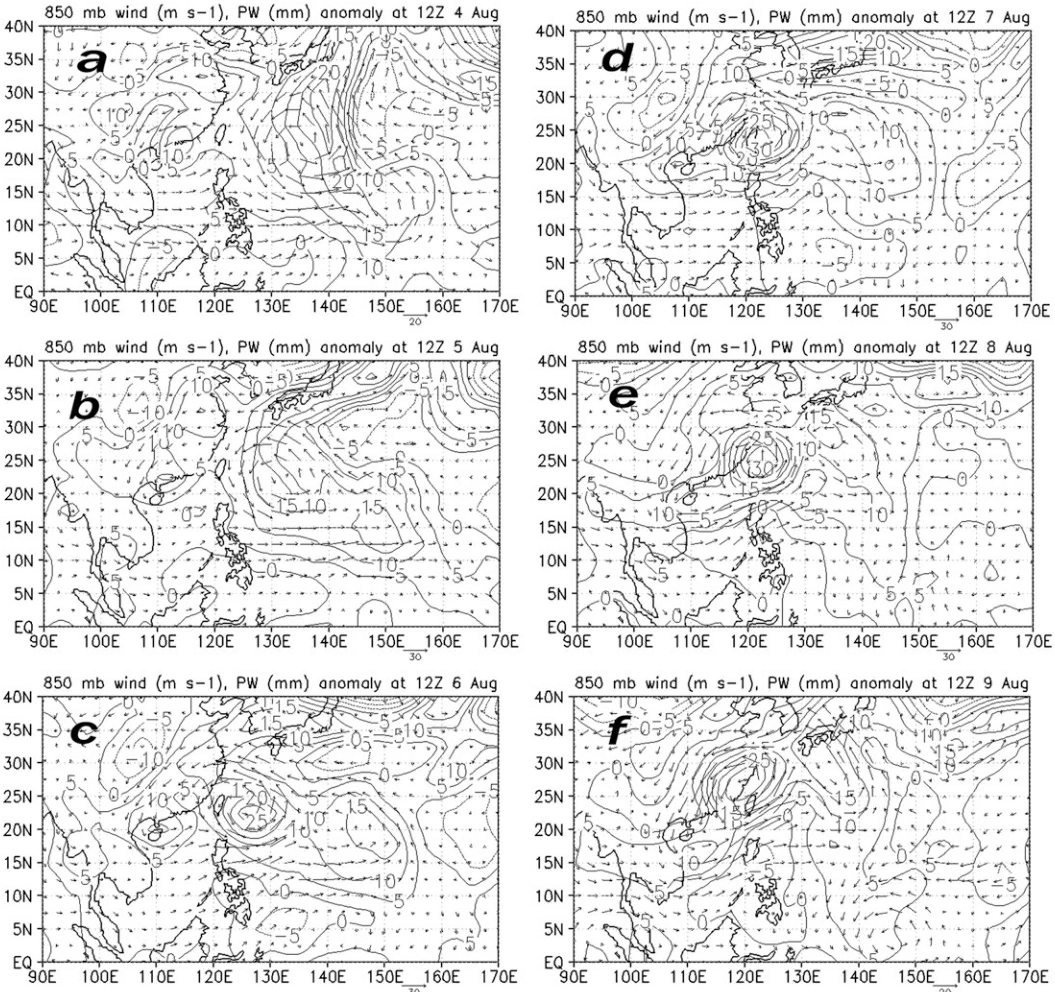

FIG. 22. FNL anomalies of 850-hPa winds (m s^{-1}) and TPW (mm) deviating from the August long-term mean at 1200 UTC (a) 4, (b) 5, (c) 6, (d) 7, (e) 8, and (f) 9 Aug 2009.

with the absolute errors in maximum wind speed and minimum surface pressure, between the observation and simulation, of less than 1 m s^{-1} and 5 hPa, respectively (Fig. 20). Because each cycle run performs an hour of simulation, the necessity for 82 cycle runs implies that it takes more than 3 days for the vortex to adapt to the WRF model and adjust to given environmental conditions and the prescribed SLP. The NT can produce a better forecast because the vortex is in balance with the large-scale environmental conditions in the model before starting model integrations. For other runs such as WB and CTRL, which lack a well-balanced initial vortex, the vortex needs to adjust to the changing environmental conditions during the first 2–3 days of model simulations. Simulation of an adjusting vortex in the midst of changing environmental conditions is likely to negatively impact the track and intensity forecasts in most cases. For the NT run, the initial TC vortex has already been spun up and is consistent with the best-track data before the start of time integration in the high-resolution model.

The development of the initial TC structure during the initialization processes for the NT scheme is given in Fig. 20. The initial vortex for the CTRL run from the NCEP/FNL analysis is weak with the radius of the maximum wind more than 4° from the storm center (Fig. 20a). During the two-step cycle runs, the radius of maximum wind decreases with increasing maximum wind speed in the model (Fig. 20) as the initial vortex adjusts to the prescribed SLP function given by (6) under the given large-scale conditions. During the cycle runs, the tilted eyewall is gradually built up and shifts toward the center of the storm. At the end of the cycle runs, the initial vortex has a minimum SLP and maximum wind speed close to observed values with the storm center at the same location as in the best-track data (Fig. 20d). It also has a well-defined eyewall with strong updrafts in the inner-core region that

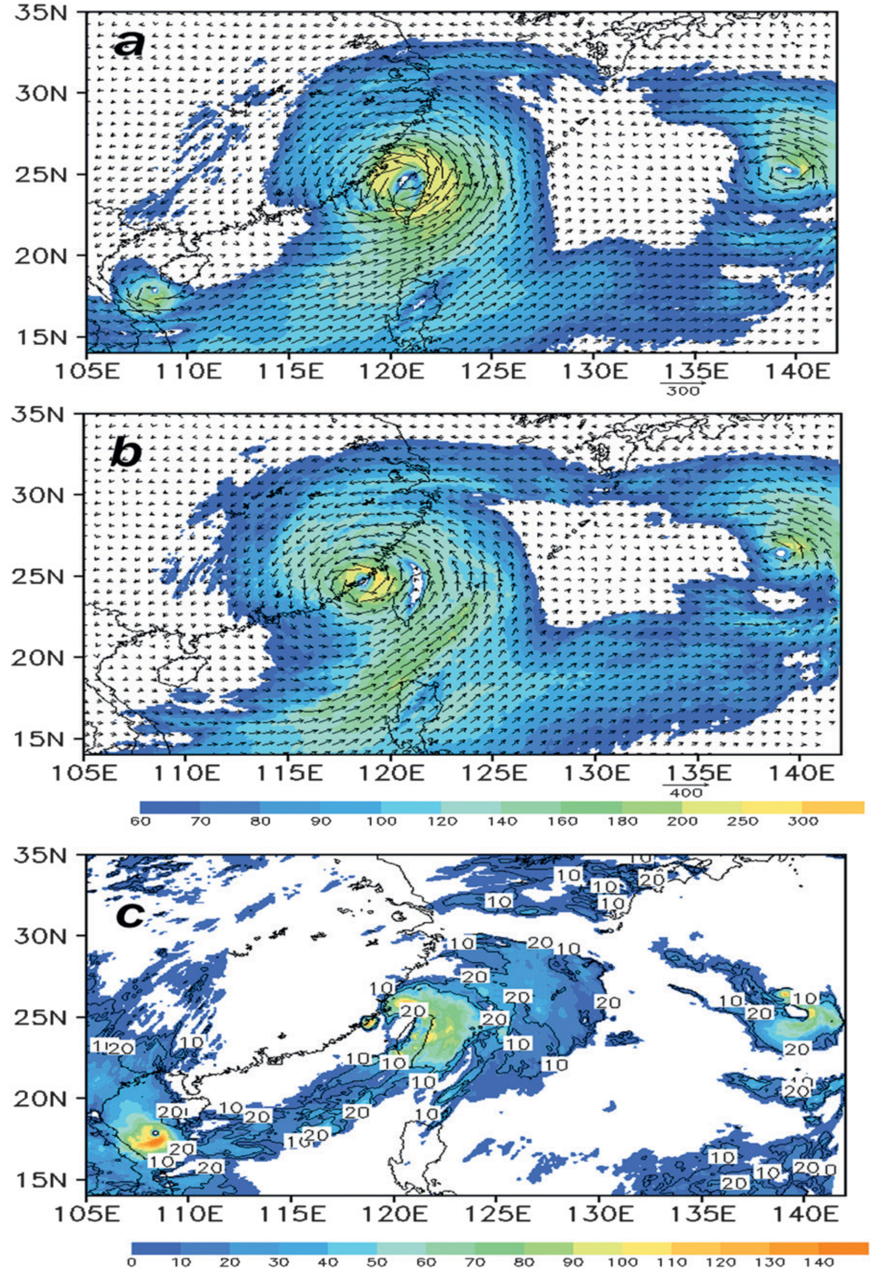

FIG. 23. The total moisture transport vector ($\times$10 kg m^{-1} s^{-1}) after 60 h of simulation valid at 1200 UTC 8 Aug 2009 (a) with Goni, (b) without Goni, and (c) the difference between with and without Goni. The contours denote 10% and 20% of the difference (with vs without Goni) compared to the total moisture transport with Goni.

resemble the observed structure of previous storms in the literature (e.g., Hawkins and Rubsam 1968; Jorgensen 1984). It appears that the latent heat release associated with the TC may play a very important role in the pressure drop during the cycle runs as the vortex adjusts to the prescribed minimum SLP. We have conducted a sensitivity test by removing the latent heat release during the two-step cycle runs. Without latent heat release, the initial vortex has difficulty in adjusting to the prescribed minimum SLP.

One of the possible impacts of this study would be to implement this scheme in operational settings in addition to using it as a research tool. To apply this scheme, we will need to know the location of the center of the storm, the minimum central pressure $P_{\min}$, and the storm size R at the model initial time from the best-track data. For this

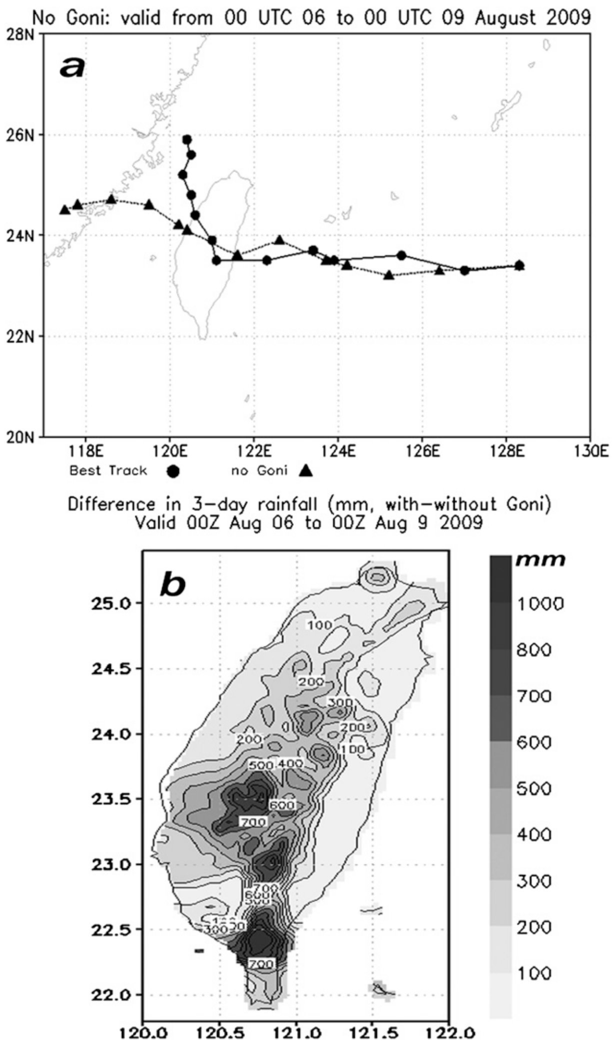

FIG. 24. (a) Morakot best track (solid line with circle) and simulated track without Goni (dashed line with triangle) valid from 0000 UTC 6 Aug to 0000 UTC 9 Aug 2009, and (b) differences in 3-day accumulated rainfall between NT and no-Goni runs (NT vs no Goni) in mm.

study, R is set as 400 km consistent with the WRF bogus scheme for comparison. The value of R can be chosen as the observed radius of 15 m s^{-1} winds. The data required for application of this scheme are readily available in real-time from the Joint Typhoon Warning Center (JTWC) best-track data. Thus, it can be tested in a real-time operational setting. However, another issue is the criteria of when to stop the cycle runs. We could end the cycle runs when the absolute errors in maximum wind speed and minimum SLP, between observation and simulation, are less than 1 m s^{-1} and 5 hPa, respectively. Normally, both conditions can be reached after about 80 cycles. In the case that 1 of the 2 conditions cannot be reached after 80 cycles, the run could be stopped at about 90 cycles. Additional tests will be performed concerning the number of cycle runs required for the initial vortex to adjust to the given large-scale conditions and to adapt to the WRF model. If additional data such as Dropwindsonde Observations for Typhoon Surveillance near the Taiwan Region (DOTSTAR; Wu et al. 2005) are available, they would provide us valuable data for improving the initial analysis for the NT scheme as well as for model verifications.

7. Factors contributing to heavy rainfall over Taiwan associated with Morakot

In this section, we would like to investigate factors important for the record-breaking heavy rainfall associated with Typhoon Morakot. FNL data are used to diagnose the large-scale patterns of wind, geopotential height, and total precipitable water (TPW) associated with Morakot. The impacts of moisture transport by another TC, Goni, and the elevated TPW associated with the monsoon gyre on localized heavy rainfall occurrences over the mountainous area that makes up southwestern Taiwan are investigated from model sensitivity tests.

During the heavy rainfall period (6–9 August), another TC, Goni, is also embedded within the monsoon gyre southwest of Morakot (Figs. 2, 3, and 21). The wind vectors in the southeast section of Goni's circulation and to the southwest of the monsoon gyre circulation are westerlies on 4 and 5 August (Figs. 21a,b) and southwesterlies from 6 to 9 August (Figs. 21c–f). At 1200 UTC 4 August, there is an area of high TPW anomalies (>10 mm) associated with Goni's circulation centered at about 20°N, 110°E (Fig. 22a). The area of high TPW anomalies associated with Goni moves southeastward from 5 to 9 August (Figs. 22b–f). During the same period, the winds associated with the monsoon gyre and Goni, within the box of 5°–10°N and 110°–125°E, shift from westerlies to southwesterlies (Fig. 21). For the two heaviest rainfall days, 7 and 8 August, the wind anomalies, from the August long-term mean in the region, are southwesterlies with anomalous speeds of about 20 m s^{-1} (Figs. 22d,e). The strong (30–40 m s^{-1}) southwesterly winds (Figs. 21d,e) bring the high TPW air (Figs. 22b–d) from low latitudes and from the vicinity of Goni's circulation toward Morakot (Fig. 22) and Taiwan. It appears that the existence of Goni within the monsoon gyre may be important for the presence of high TPW air moving toward the island of Taiwan.

To investigate the role of Goni on moisture transport toward the Morakot circulation, a simulation without Typhoon Goni (NGN) in the initial conditions is performed and compared with the case run with Goni (WGN). Water vapor transport vectors ($\mathbf{Q}$; kg m^{-1} s^{-1}) for WGN, NGN, and the difference between WGN and

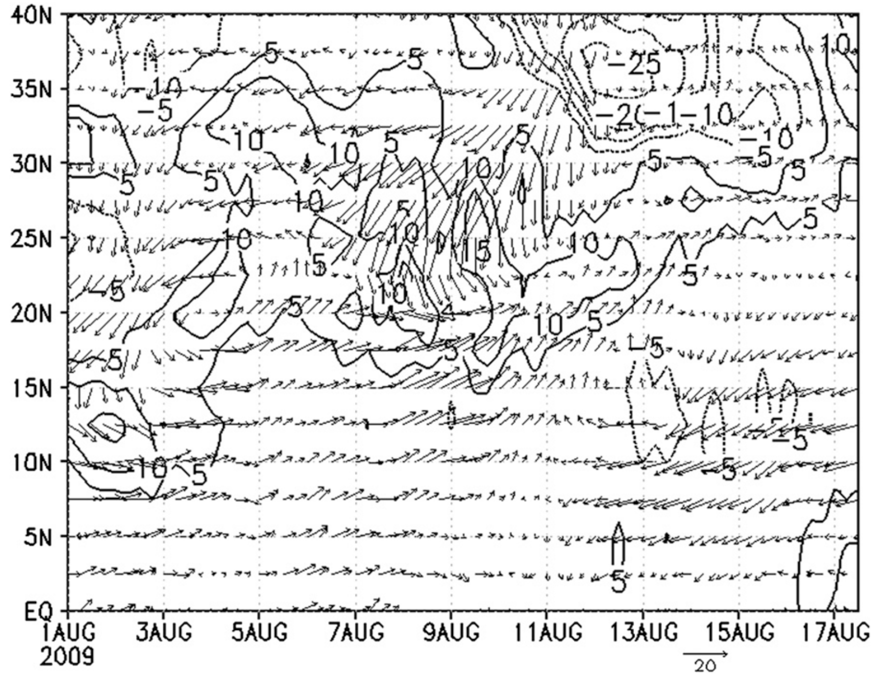

FIG. 25. Time–latitude cross section along 115°E of FNL 850-hPa wind anomalies (m s^{-1}) and precipitable water anomalies (contoured; mm) from the August long-term mean.

NGN (WGN − NGN) are computed, following Smirnov and Moore (1999), as

$$\mathbf{Q} = \frac{1}{g}\int_0^{p_0} q\mathbf{V}\,dp, \tag{10}$$

where q (kg kg^{-1}) is the water vapor mixing ratio, $\mathbf{V}$ (m s^{-1}) is the horizontal wind vector, p is the pressure, and p_0 is the surface pressure.

The moisture transport vectors ($\times$10 kg m^{-1} s^{-1}) for the WGN run at 60 h of integration, valid at 1200 UTC 8 August 2009, show that there are three areas of high values of moisture transport associated with three typhoons including Morakot, Goni, and Etau (Fig. 23a). The differences in moisture transport (WGN − NGN) demonstrate that Typhoon Goni induced a moisture transport channel from south of Goni and the monsoon gyre toward southern Taiwan (Fig. 23c). The magnitude of Goni-induced moisture transport within the channel contributes to 10%–20% of the total moisture transport in the WGN run for the same region.

When Typhoon Goni is removed from the initial conditions, the simulated track of Typhoon Morakot is slightly changed and Morakot moves to the west of the best track (Fig. 24a). With the reduced moisture transport by Typhoon Goni and the change in simulated track, the simulated rainfall in the NGN run (Fig. 24b) is 500–900 mm less over southwestern Taiwan than for the WGN run. It is evident that the removal of Goni affects the track of Morakot with reduced moisture transport toward the area of southern Taiwan resulting in much less rainfall over those mountainous areas.

Figure 25 shows that during the period of heavy rainfall (e.g., 6–9 August) in addition to southwesterly winds associated with the monsoon gyre and Goni circulations from 10° to 20°N, northwesterly winds associated with the northwestern part of the monsoon gyre and Morakot circulations are also important (Figs. 22 and 25). During 6–9 August, there is another typhoon named Etau embedded within the monsoon gyre to the east of Morakot (Figs. 21c–e) with an area of high TPW anomalies (>10 mm; Figs. 22c,d) east and northeast of Morakot. Strong (>20 m s^{-1}) southeasterly winds along the east-northeastern periphery of the monsoon gyre (Figs. 21c–f) bring high TPW air (Figs. 22d–f) toward the south China coast. The high TPW air then moves with the northwesterly winds, west of the Morakot circulation, toward southwest Taiwan.

Jiang et al. (2008a) use the water vapor budget to examine the relationship between heavy rainfall and environmental conditions for Hurricane Isidore (2002). They state that horizontal moisture convergence and ocean surface fluxes are the main factors influencing the maintenance of intense rainfall. They also suggest that adding TPW into the current forecast scheme will result in better TC rainfall prediction (Jiang et al. 2008b). A sensitivity test,

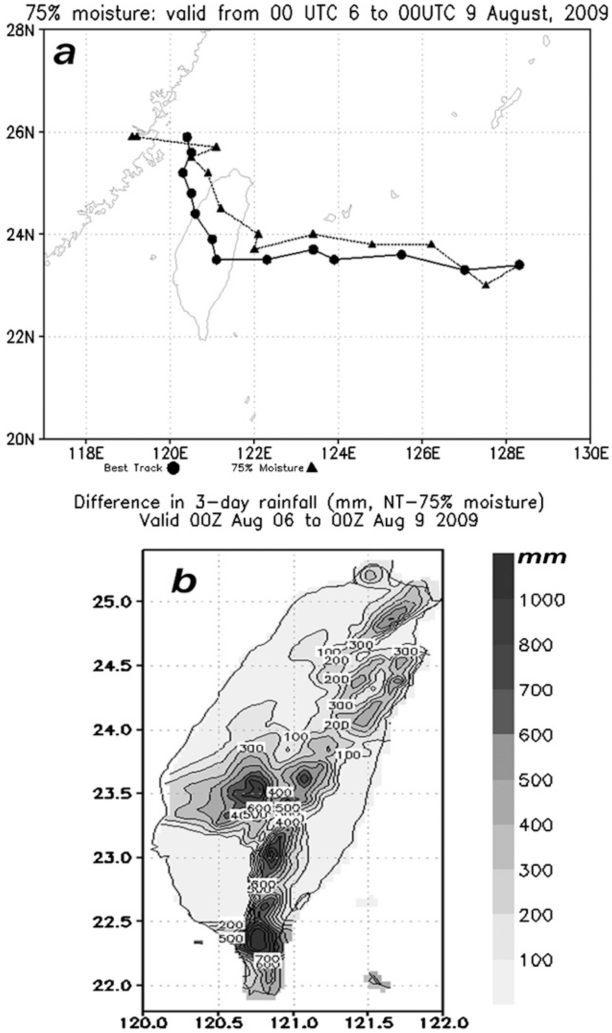

FIG. 26. (a) Morakot best track (solid line with circle) and simulated track in which the mixing ratio is reduced to 75% of the value in the NT run (dashed line with triangle) valid from 0000 UTC 6 Aug to 0000 UTC 9 Aug 2009 and (b) differences in 3-day accumulated rainfall between NT and 75% moisture runs (NT vs 75% moisture) in mm.

with mixing ratio at the time of initialization reduced to 75% of the global analysis, is performed. Figure 26a shows that with reduction in moisture, the simulated track (Fig. 26a) is not significantly changed as compared to the NT run (Fig. 13c). With reduced moisture, simulated rainfall over Taiwan is much less than in the NT run (Fig. 26b). Over the two regions of observed local rainfall maxima near 22.8° and 23.5°N, the simulated rainfall is reduced by about 300–700 mm (Fig. 26b) as compared with the NT run.

To investigate the role of terrain effects on the heavy rainfall event, a vertical cross section of winds at 1200 UTC 8 August 2009, along 23.5°N at which a maximum in local rainfall was observed, is constructed (Fig. 27). The day with the largest observed 24-h accumulated rainfall during the 5-day period when Taiwan is feeling the influences of Morakot is 8 August. At 1200 UTC 8 August 2009, there are strong low-level winds (>40 m s^{-1}) impinging on the western slopes of southwestern Taiwan (Fig. 27a). Strong horizontal winds bring moist-laden air toward the mountain areas which is one of the important factors for orographically enhanced precipitation in the region (Chiao and Lin 2003). The orographic lifting enhanced by latent heat release results in strong upward motions as found by Wu et al. (2002).

The convergence zone between the Morakot circulation and the southwest monsoon over southeast Taiwan and offshore is also one of the important factors for heavy rainfall occurrence. Both simulated (Fig. 11b) and observed (Fig. 11a) radar reflectivities show that at 1200 UTC 8 August 2009, there is a band of high reflectivities at ~23.5°N where the simulated Morakot circulation and southwest monsoon flow converge. The continuous eastward movement of the simulated cells embedded in the band with the westerly winds resulted in a simulated local rainfall maximum over the mountainous area at ~23.5°N (Fig. 12b) in the NT run consistent with observations (Fig. 12a). Note that with a better track forecast, this convergence zone and the associated high radar reflectivity and rainband are well simulated in the NT run with a local rainfall maximum around 23.5°N over the mountainous area of southern Taiwan (Fig. 12b). In contrast, these features, and the local rainfall maximum there, are missed in both the CTRL and BW runs (Figs. 12c,d). The vertical cross section along 119.5°E shows that near 23.5°N, the simulated meridional winds converge from two opposite directions with positive values to the south, related to the monsoonal flow, and negative values to the north related to Morakot's circulations (Fig. 28a). The convergence induces strong vertical motions of over 4 m s^{-1} at about 23.3°N over the open ocean west of Taiwan (Fig. 28b).

The slow movement of Morakot over Taiwan (Fig. 2) is favorable for prolonged heavy rainfall. Morakot's center stayed over Taiwan for almost a day (Figs. 2 and 21d,e). In addition to its slow translational movement, Morakot has a relatively large size (Fig. 21a). With its large size and slow movement, the Morakot circulation was able to affect Taiwan for more than 5 days (Figs. 21b–f). Persistent orographic lifting of the warm, moist flow by the broad westerly wind component in the monsoon gyre and Morakot's circulation (Figs. 21c–f) is one of the main factors for the development of heavy rainfall. However, if the very moist air associated with Goni and Etau embedded within the monsoon gyre did not exist, and if the very moist air associated with the southwest monsoon flow were not present and if Morakot did not have a relatively large size and slow movement the record rainfall over Taiwan probably would

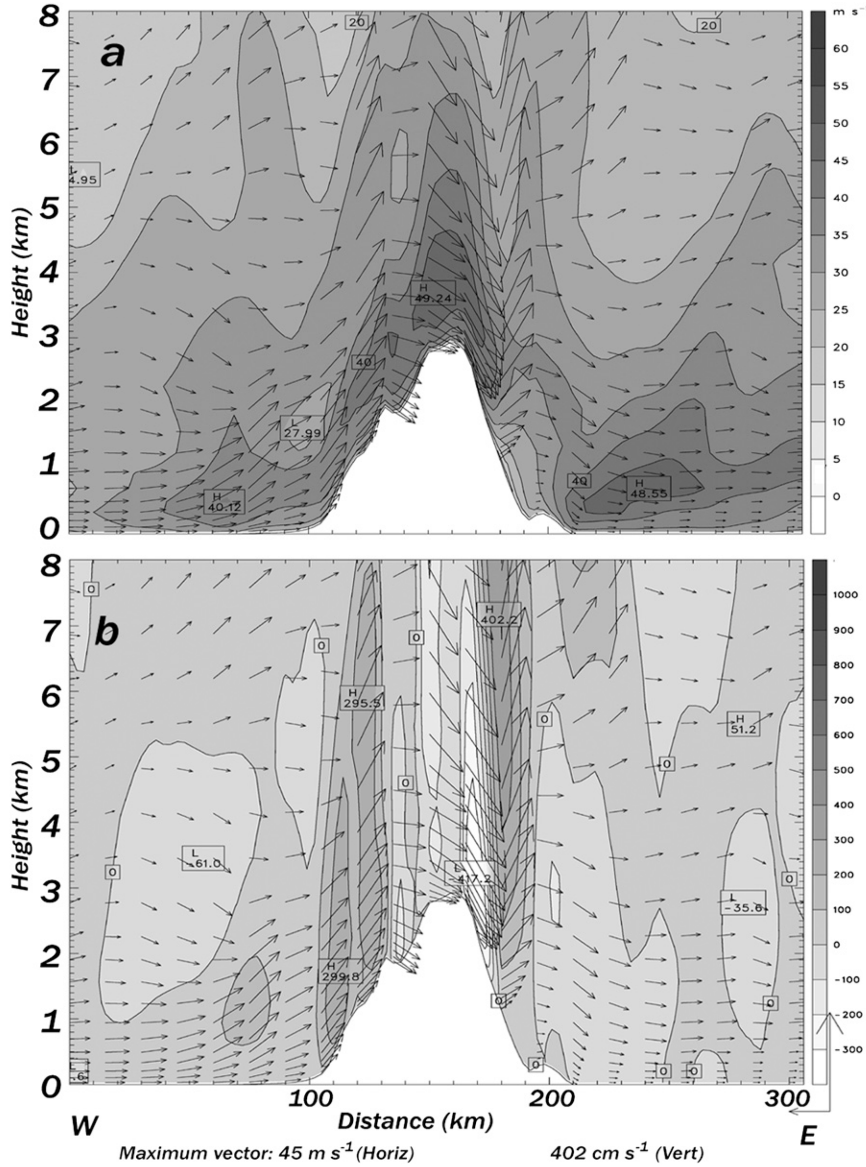

FIG. 27. Vertical cross section along 23.5°N, from 119.5° to 122.5°E, at the 60th hour of simulation for (a) total wind speed (shaded) and total wind vector (m s^{-1}), and (b) vertical velocity (shaded, cm s^{-1}) and total wind vector (m s^{-1}), valid at 1200 UTC 8 Aug 2009.

not have occurred. A schematic diagram showing the circulations of the three tropical storms embedded within the monsoon gyre, with elevated TPW, is given in Fig. 29. The flows that help to bring moisture and impinge on the western slopes of southern Taiwan in the southwestern quadrant of the Morakot circulation are highlighted by small arrows with waving tails.

8. Summary and discussion

In this work, a model self-bogus vortex is constructed by model cycle runs using the WRF model version 3 to provide high-resolution initial conditions for tropical cyclone simulations (NT). During the cycle runs, only SLP is forced at the first time step of each cycle run by an empirical profile, assuming that in a short period (~1 h) the TC moves but its structure does not change significantly. The vortex after 1 h of model simulation is used to construct the vortex structure at the initial condition for the next cycle run. After about eighty 1-h cycle runs, the tropical cyclone structure is well established under the given large-scale conditions.

Three separate runs initialized at 0000 UTC 6 August 2009 with three different initial conditions including the

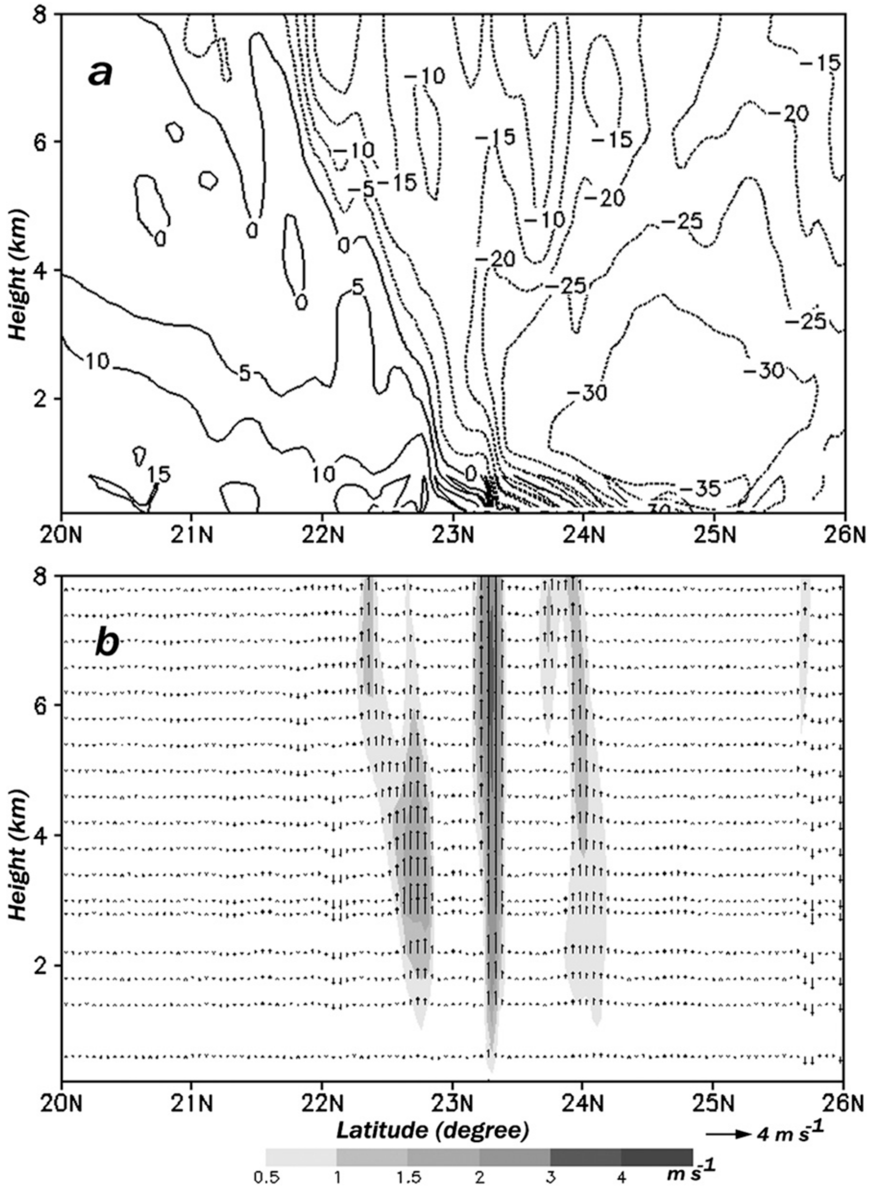

FIG. 28. Longitude–vertical cross section along 119.5°E of (a) simulated meridional winds (contour, 5 m s^{-1} interval) and (b) the simulated vertical wind vector (vector, m s^{-1}) and vertical velocity (shaded, m s^{-1}) at 1200 UTC (60th h of simulation) 8 Aug 2009.

CTRL, WB, and NT runs were performed for Typhoon Morakot (2009) to investigate the impacts of TC initialization on TC forecasts. Without vortex initialization, the simulated vortex in the CTRL run is too weak. Maximum wind speed for the CTRL run at the initial time, of about 18 m s^{-1}, is much weaker than what is observed (~33.5 m s^{-1}). The radius of maximum wind in the CTRL is about 4°, which is too large and unrealistic. The WRF bogus scheme (WB) can reasonably generate some features of the TC including lower minimum SLP, stronger winds in the TC core at the model initial time, and better minimum SLP up to 48 h of simulation. However, there are several shortcomings in the WRF bogus package including the fact that the altitude of the warm core is too low, that it produces stronger winds than in the global analysis at large radii away from the TC center, and that the simulated maximum wind speed is significantly weaker than observed. The NT run shows advantages over both the CTRL and WB cases in generating realistic vortex features at the initial time including SLP, winds, warm core, TC size, asymmetric rainband structure, and meteorological fields away from the observed TC center consistent with

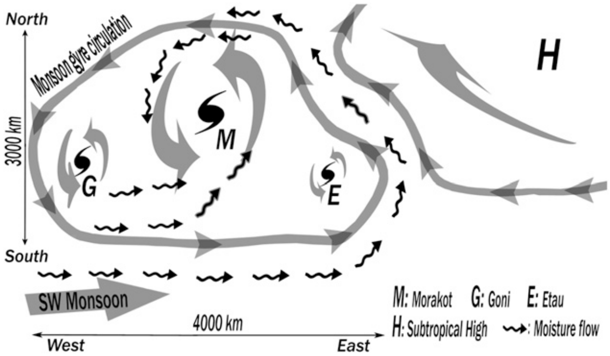

FIG. 29. Schematic diagram of Morakot embedded within a monsoon gyre circulation and the flows of moisture laden air (highlighted with small arrows with waving tails) associated with Morakot as the flow with a westerly component impinges on the western slope of southern Taiwan. Southern Taiwan is in the southwestern quadrant of Morakot's circulations during the period with heavy precipitation (7–9 Aug 2009).

the global analysis. The NT run also shows improvements in simulating TC structure, intensity, low-level winds, radar reflectivities, track, and rainfall as compared to both the CTRL and WB runs.

Sensitivity tests were performed with error statistics to examine the ability of the CTRL, WB, and NT runs in simulating track, intensity, and rainfall for Morakot. With each type of initialization, seven 48-h model runs were performed with initialization at every 12 h from 0000 UTC 5 August to 0000 UTC 8 August. For the NT run, when the TC center is located within less than 400 km of the nearest coast (from 0000 UTC 7 August), no cycle runs are performed. In this case, the 12-h integrated vortex from the previous run, initialized 12 h earlier, is used as the initial vortex for current simulation. Prior to 0000 UTC 7 August, the full NT initialization scheme described in section 2 is used. For the Morakot case, track simulations between 24 and 36 h in the WB run are worse than in the CTRL. The NT run shows significant improvements in track and intensity simulations during the period (0000 UTC 5 August–0000 UTC 10 August) as compared to the other two runs. The mean 24-h track errors for the seven runs are 100, 130, and 60 km for the CTRL, WB, and NT runs, respectively. The mean 48-h track errors are 250, 190, and 80 km for the CTRL, WB, and NT runs, respectively. Mean 24-h maximum absolute wind speed errors are 8, 6.5, and 3.5 m s^{-1} for the CTRL, WB, and NT runs, respectively. Mean 48-h maximum absolute wind speed errors are 7, 6, and 2 m s^{-1} for the CTRL, WB, and NT runs, respectively. Mean absolute SLP errors at 24 and 48 h of simulation in the NT run are about ⅓ and ½ of that in the CTRL and the WB runs, respectively.

The NT run shows that it takes more than 3 days for the typhoon vortex to adapt to the WRF model and adjust to the given environmental conditions and a prescribed SLP. The initial TC vortex in the NT run has already been spun up before model integration resulting in better TC track, intensity, and rainfall simulations. For other runs, such as WB and CTRL, the unbalanced initial vortex needs to adjust to the changing environmental conditions during the first 2–3 days of model simulations. Simulation of an adjusting vortex in changing environmental conditions will likely have negative impacts on the track, intensity, and rainfall forecasts in most cases.

With better initial conditions, the NT run produces better rainfall simulation over the open ocean as compared to the other two runs because rainfall and radar reflectivity patterns associated with the eyewall and asymmetric rainbands are better simulated in the NT run. The model is capable of simulating heavy orographic precipitation over southern Taiwan for all three different types of model initializations reasonably well, however, only the NT run with an improved track forecast is capable of simulating the high reflectivity band associated with the convergence zone between Morakot and the southwest monsoon. In addition to the slow movement and relatively large size of Morakot, Typhoons Goni and Etau were embedded in a moist (TPW anomalies >10 mm) monsoon gyre. During 3 days of the heaviest rainfall, 7–9 August, Taiwan is in the southwestern quadrant of Morakot. The increase in the southwesterlies associated with the combined circulations of Goni, Morakot, and the monsoon gyre to the southwest of Taiwan and the increase in northwesterlies associated with the combined Morakot–monsoon gyre circulations to the northwest of the Taiwan Strait help to bring a persistent moisture-laden westerly wind component that impinges on the high mountain slopes of southern Taiwan.

Acknowledgments. This work was funded by the Pacific Disaster Center, Kihei, Hawaii. We also would like to thank the USDA Forest Service; the University of Hawaii/Maui High Performance Computing Center (UH/MHPCC) for helping to fund this research; the Joint Institute of Marine and Atmospheric Research (JMAR)/NOAA for funding the publication costs; Profs. F. F. Jin, P.-S. Chu, D. E. Stevens, and K. F. Cheung for their comments; and Mei-Yu Chang and Dr. S.-C. Lin of Central Weather Bureau, Taiwan, for the land surface data and rainfall data used in this research.

REFERENCES

Bender, M. A., R. E. Tuleya, and Y. Kurihara, 1985: A numerical study of the effect of a mountain range on a landfalling tropical cyclone. *Mon. Wea. Rev.,* **113,** 567–582.

——, ——, and ——, 1987: A numerical study of the effect of island terrain on tropical cyclones. *Mon. Wea. Rev.,* **115,** 130–155.

——, R. Ross, R. E. Tuleya, and Y. Kurihara, 1993: Improvements in tropical cyclone track and intensity forecasts using the GFDL initialization system. *Mon. Wea. Rev.,* **121,** 2046–2061.

Brand, S., and J. W. Blelloch, 1974: Changes in the characteristics of typhoons crossing the island of Taiwan. *Mon. Wea. Rev.,* **102,** 708–713.

Chan, J. C.-L., and R. T. Williams, 1987: Analytical and numerical study of the beta-effect in tropical cyclone motion. Part I: Zero mean flow. *J. Atmos. Sci.,* **44,** 1257–1265.

Chang, S. W., 1982: The orographic effects induced by an island mountain range on propagating tropical cyclones. *Mon. Wea. Rev.,* **110,** 1255–1270.

Chen, C.-S., Y.-L. Chen, W.-C. Chen, and P.-L. Lin, 2007: The statistics of heavy rainfall occurrences in Taiwan. *Wea. Forecasting,* **22,** 981–1002.

Chen, F., and J. Dudhia, 2001: Coupling an advanced land surface-hydrology model with the Penn State–NCAR MM5 modeling system. Part I: Model implementation and sensitivity. *Mon. Wea. Rev.,* **129,** 569–585.

Cheung, K. K. W., L.-R. Huang, and C.-S. Lee, 2008: Characteristics of rainfall during tropical cyclone periods in Taiwan. *Nat. Hazards Earth Syst. Sci.,* **8,** 1463–1474.

Chiao, S., and Y.-L. Lin, 2003: Numerical modeling of an orographically induced precipitation event associated with Tropical Storm Rachel over Taiwan. *Wea. Forecasting,* **18,** 325–344.

Chou, K.-H., and C.-C. Wu, 2008: Typhoon initialization in a mesoscale model—Combination of the bogused vortex and the dropwindsonde data in DOTSTAR. *Mon. Wea. Rev.,* **136,** 865–879.

Davidson, N. E., and H. C. Weber, 2000: The BMRC high-resolution tropical cyclone prediction system: TC-LAPS. *Mon. Wea. Rev.,* **128,** 1245–1265.

Davis, C. A., and S. Low-Nam, 2001: The NCAR–AFWA tropical cyclone bogussing scheme: A report prepared for the Air Force Weather Agency (AFWA). National Center for Atmospheric Research, 13 pp. [Available online at http://www.mmm.ucar.edu/mm5/mm5v3/tc-report.pdf.]

Dudhia, J., 1989: Numerical study of convection observed during the winter monsoon experiment using a mesoscale two-dimensional model. *J. Atmos. Sci.,* **46,** 3077–3107.

Ferrier, B. S., Y. Jin, Y. Lin, T. Black, E. Rogers, and G. DiMego, 2002: Implementation of a new grid-scale cloud and precipitation scheme in the NCEP Eta model. Preprints, *15th Conf. on Numerical Weather Prediction,* San Antonio, TX, Amer. Meteor. Soc., 280–283.

Fujita, T., 1952: Pressure distribution within typhoon. *Geophys. Mag.,* **23,** 437–451.

Hawkins, H. F., and D. T. Rubsam, 1968: Hurricane Hilda, 1964 II. Structure and budgets of the hurricanes on October 1, 1964. *Mon. Wea. Rev.,* **96,** 617–636.

Holland, G. J., 1980: An analytic model of the wind and pressure profiles in a hurricane. *Mon. Wea. Rev.,* **108,** 1212–1218.

Hong, C.-C., H.-H. Hsu, M.-Y. Lee, and J.-L. Kuo, 2010: Role of submonthly disturbance and 40-50-day ISO on the extreme rainfall event associated with Typhoon Morakot (2009) in Southern Taiwan. *Geophys. Res. Lett.,* **37,** L08805, doi:10.1029/2010GL042761.

Iwasaki, T., H. Nakano, and M. Sugi, 1987: The performance of a typhoon track prediction model with convective parameterization. *J. Meteor. Soc. Japan,* **65,** 555–570.

Janjic, Z. I., 1994: The step–mountain eta coordinate model: Further developments of the convection, viscous sublayer, and turbulence closure schemes. *Mon. Wea. Rev.,* **122,** 927–945.

——, 2000: Comments on "Development and evaluation of a convection scheme for use in climate models." *J. Atmos. Sci.,* **57,** 3686.

Jian, G.-J., C.-S. Lee, and G. T.-J. Chen, 2006: Numerical simulation of Typhoon Dot (1990) during TCM-90: The discontinuous track across Taiwan. *Terr. Atmos. Oceanic Sci.,* **17,** 23–52.

Jiang, H., J. B. Halverson, J. Simpson, and E. J. Zipser, 2008a: On the differences in storm rainfall from Hurricanes Isidore and Lili. Part II: Water budget. *Wea. Forecasting,* **23,** 44–61.

——, ——, and E. J. Zipser, 2008b: Effects of environmental moisture on tropical cyclone precipitation: Land/ocean difference. *Geophys. Res. Lett.,* **35,** L17806, doi:10.1029/2008GL034658.

Jorgensen, D. P., 1984: Mesoscale and convective-scale characteristics of mature hurricanes. Part II: Inner-core structure of Hurricane Allen (1980). *J. Atmos. Sci.,* **41,** 1287–1311.

Kurihara, Y., M. A. Bender, R. E. Tuleya, and R. J. Ross, 1990: Prediction experiments of Hurricane Gloria (1985) using a multiply nested movable mesh model. *Mon. Wea. Rev.,* **118,** 2185–2198.

——, ——, and R. J. Ross, 1993: An initialization scheme of hurricane models by vortex specification. *Mon. Wea. Rev.,* **121,** 2030–2045.

Kwon, I.-H., and H.-B. Cheong, 2010: Tropical cyclone initialization with spherical high-order filter and idealized three-dimensional bogus vortex. *Mon. Wea. Rev.,* **138,** 1344–1367.

Lander, M. A., 1994: Description of a monsoon gyre and its effect on the tropical cyclones in the Western North Pacific during August 1991. *Wea. Forecasting,* **9,** 640–654.

Lin, Y. L., D. B. Ensley, and S. Chiao, 2002: Orographic influences on rainfall and track deflection associated with the passage of a tropical cyclone. *Mon. Wea. Rev.,* **130,** 2929–2950.

Liu, Y., D.-L. Zhang, and M. K. Yau, 1997: A multiscale numerical study of Hurricane Andrew (1992). Part I: Explicit simulation and verification. *Mon. Wea. Rev.,* **125,** 3073–3093.

Mathur, M. B., 1991: The national meteorological center's quasi-Lagrangian model for hurricane prediction. *Mon. Wea. Rev.,* **119,** 1419–1447.

Mlawer, E. J., S. J. Taubman, P. D. Brown, and M. J. Iacono, 1997: Radiative transfer for inhomogeneous atmospheres: RRTM, a validated correlated-k model for the longwave. *J. Geophys. Res.,* **102,** 16 663–16 682.

Monin, A. S., and A. M. Obukhov, 1954: Basic laws of turbulent mixing in the surface layer of the atmosphere. *Contrib. Geophys. Inst. Acad. Sci., USSR,* **151,** 163–187.

Noh, Y., W. G. Cheon, S. Y. Hong, and S. Raasch, 2003: Improvement of the K-profile model for the planetary boundary layer based on large eddy simulation data. *Bound.-Layer Meteor.,* **107,** 421–427.

Pu, Z. X., and S. A. Braun, 2001: Evaluation of bogus vortex techniques with fou-dimensional variational data assimilation. *Mon. Wea. Rev.,* **129,** 2023–2039.

Ross, R., and Y. Kurihara, 1992: A simplified scheme to simulate asymmetries due to the beta effect in barotropic vortices. *J. Atmos. Sci.,* **49,** 1620–1628.

Skamarock, W. C., J. B. Klemp, J. Dudhia, D. O. Gill, D. M. Barker, W. Wang, and J. G. Powers, 2005: A description of the Advanced Research WRF version 2. NCAR Tech. Note TN-468 STR, 88 pp.

Smirnov, V. V., and G. W. K. Moore, 1999: Spatial and temporal structure of atmospheric water vapor transport in the Mackenzie River basin. *J. Climate,* **12,** 681–696.

Viltard, N., C. Burlaud, and C. D. Kummerow, 2006: Rain retrieval from TMI brightness temperature measurements using a TRMM PR-based database. *J. Appl. Meteor. Climatol.,* **45,** 455–466.

Wang, D., X. Liang, Y. Zhao, and B. Wang, 2008: A comparison of two tropical cyclone bogussing schemes. *Wea. Forecasting,* **23,** 194–204.

Wu, C.-C., 2001: Numerical simulation of Typhoon Gladys (1994) and its interaction with Taiwan terrain using the GFDL hurricane model. *Mon. Wea. Rev.,* **129,** 1533–1549.

——, and Y.-H. Kuo, 1999: Typhoons affecting Taiwan: Current understanding and future challenges. *Bull. Amer. Meteor. Soc.,* **80,** 67–80.

——, T.-H. Yen, Y.-H. Kuo, and W. Wang, 2002: Rainfall simulation associated with Typhoon Herb (1996) near Taiwan. Part I: The topographic effect. *Wea. Forecasting,* **17,** 1001–1015.

——, and Coauthors, 2005: Dropwindsonde Observations for Typhoon Surveillance near the Taiwan Region (DOTSTAR): An overview. *Bull. Amer. Meteor. Soc.,* **86,** 787–790.

——, K.-H. Chou, Y. Wang, and Y.-H. Kuo, 2006: Tropical cyclone initialization and prediction based on four-dimensional variational data assimilation. *J. Atmos. Sci.,* **63,** 2383–2395.

——, K. K. W. Cheung, and Y. Y. Lo, 2009: Numerical study of the rainfall event due to the interaction of Typhoon Babs (1998) and the northeasterly monsoon. *Mon. Wea. Rev.,* **137,** 2049–2064.

Yeh, T.-C., and R. L. Elsberry, 1993a: Interaction of typhoons with the Taiwan orography. Part I: Upstream track deflections. *Mon. Wea. Rev.,* **121,** 3193–3212.

——, and ——, 1993b: Interaction of typhoons with the Taiwan orography. Part II: Continuous and discontinuous tracks across the island. *Mon. Wea. Rev.,* **121,** 3213–3233.

Zhang, X., Q. Xiao, and P. J. Fitzpatrick, 2007: The impact of multisatellite data on the initialization and simulation of Hurricane Lili's (2002) rapid weakening phase. *Mon. Wea. Rev.,* **135,** 526–548.

Zhang, Y., Y.-L. Chen, S.-Y. Hong, H.-M. H. Juang, and K. Kodama, 2005: Validation of the coupled NCEP mesoscale spectral model and an advanced land surface model over the Hawaiian Islands. Part I: Summer trade wind conditions and a heavy rainfall event. *Wea. Forecasting,* **20,** 847–872.

Zhao, Y., B. Wang, and Y. Wang, 2007: Initialization and simulation of a landfalling typhoon using a variational bogus mapped data assimilation (BMDA). *Meteor. Atmos. Phys.,* **98,** 269–282.

Zou, X., and Q. Xiao, 2000: Studies on the initialization and simulation of a mature hurricane using a variational bogus data assimilation scheme. *J. Atmos. Sci.,* **57,** 836–860.